製造 (Production)：材料の受け取りから配給までIND製品の準備に含まれるすべての作業．加工，保管，梱包，ラベル添付，試験検査，品質管理も含む

スクリーニング試験 (Screening study)：探索的IND申請の下で実施されるスクリーニング試験は，従来のIND申請における臨床開発に付け加え，より有効な化合物や製法を選別するために活性部分の特性を比較することを目的としている．

仕様 (specification)：検査リスト，分析手順の出典，妥当な承認基準（数的な限界・範囲やその他の試験基準）．これは，薬の製剤原薬や製剤が，目的とされた使用において許容可能と見なされるために満たされる必要がある一連の基準を明確にする．「仕様を満たす」とは，物質がそこに挙げられた分析手順に従って試験された際，挙げられた承認基準に合致することを意味している．

スポンサー (Sponsor)：臨床試験に対し責任を負い，これを主導する者[*30]．

品質管理単位 (Quality Unit)：品質管理責任を果たす組織単位．組織の大きさと構造によって，これが独立したQC（品質管理）単位の場合もあれば，一個人もしくはグループの形である場合もある．

[*30] 訳註：多くの場合は製薬企業．いわゆる医師主導型治験や臨床試験では，医師あるいは研究者を指す．

文 献

1. FDA Guidance for Industry *Content and Format of Investigational New Drug Applicatons (INDs) for Phase 1 Studies of Drugs, Including Well-Characterized, Therapeutic, Biotechnology-derived Products.* [*31]
2. FDA Draft Guidance for Rreviewers : *Instructions and Template for Chemistry, Manufacturing, and Control (CMC) Reviewers of Human Somatic Cell Therapy Investigational New Drug Applications (INDs)*, August 15, 2003 [*32]
3. FDA Draft Guidance for FDA Review Staff and Sponsors : *Content and Review of Chemistry, Manufacturing, and Control (CMC) Information for Human Gene Therapy Investigational New Drug Applications (INDs)*, November 8, 2004. [*33]
4. FDA Guidance for Industry: *Q7A Good Manufacturing Practice Guidance for Active Pharmaceutical Ingredients*, Section 19. [*34]

*31 訳註：http://www.fda.gov/cder/guidance/clin2.pdf
*32 訳註：http://www.fda.gov/CbER/gdlns/cmcsomcell.pdf
*33 訳註：http://www.fda.gov/CbER/gdlns/gtindcmc.pdf
*34 訳註：http://www.fda.gov/cder/guidance/4286fnl.pdf

STEM CELLS®

TRANSLATIONAL AND CLINICAL RESEARCH

HOX Decoy Peptide Enhances the Ex Vivo Expansion of Human Umbilical Cord Blood CD34$^+$ Hematopoietic Stem Cells/Hematopoietic Progenitor Cells

HIROKAZU TANAKA,[a,b] ITARU MATSUMURA,[b] KIMINARI ITOH,[a] ASAKO HATSUYAMA,[a] MASAYUKI SHIKAMURA,[a] YUSUKE SATOH,[b] TOSHIO HEIKE,[c] TATSUTOSHI NAKAHATA,[c] YUZURU KANAKURA[b]

[a]Department of Regenerative Medicine, Institute of Biomedical Research and Innovation, Kobe, Japan; [b]Department of Hematology and Oncology, Osaka University Graduate School of Medicine, Osaka, Japan; [c]Department of Pediatrics, Graduate School of Medicine, Kyoto University, Kyoto, Japan

Key Words. Ex vivo expansion • Hematopoietic stem/progenitor cells • HOX • Peptide mimetics

ABSTRACT

HOX transcription factors play important roles in the self-renewal of hematopoietic cells. HOX proteins interact with the non-HOX homeobox protein PBX1 to regulate, both positively and negatively, the expression of target genes. In this study, we synthesized a decoy peptide containing the YPWM motif from HOX proteins (decoy HOX [decHOX]), which was predicted to act as a HOX mimetic, and analyzed its effects on self-renewal of human cord blood CD34$^+$ cells. We were able to deliver decHOX into approximately 70% of CD34$^+$ cells. By examining the expression of HOX target genes c-*myc* and *p21$^{waf1/cip1}$*, we confirmed that decHOX nhanced HOX functions. After 7 days of culture in serum-free medium containing a cytokine cocktail, cultures treated with decHOX had approximately twofold-increased numbers of CD34$^+$ cells and primitive multipotent progenitor cells compared with control cells. Furthermore, decHOX-treated cells reconstituted hematopoiesis in nonobese diabetic/severe combined immunodeficiency mice more rapidly and more effectively (more than twofold greater efficiency, as determined by a limiting dilution method) than control cells. decHOX-treated cells were also able to repopulate secondary recipients. Together, these results indicate that in combination with growth factors and/or other approaches, decHOX might be a useful new tool for the ex vivo expansion of hematopoietic stem/progenitor cells.
STEM CELLS *2006;24:2592–2602*

INTRODUCTION

Human umbilical cord blood (CB) is a useful source of hematopoietic stem cells (HSCs) for transplantation. In fact, during the last few years, an increasing number of patients have received CB transplants [1]. However, clinical applications of CB are inevitably limited by the fact that the number of HSCs in each CB sample is insufficient for many adult patients. Also, compared with transplantation of HSCs from the bone marrow or HSCs mobilized into peripheral blood, the recovery of hematopoiesis is rather delayed in patients receiving CB transplants, partly because of the insufficient number of transplanted HSCs and progenitor cells and the persistent quiescence of CB HSCs that sometimes accompanies lethal complications [1]. Therefore, it is of particular interest to expand CB HSCs ex vivo and to develop strategies for hastening hematopoietic recovery after CB transplantation in vivo [2]. Regarding strategies for ex vivo expansion, the most important problem is to preserve the functions and properties of HSCs, that is, self-renewal and multipotency, during culturing. At present, the use of cytokines is the most promising and practical strategy for this purpose. To establish the culture conditions most suitable for expansion of HSCs, a number of investigators have used various cytokine combinations [2, 3]. When their effects were compared by long-term reconstitution assays in transplanted mice, the combination of stem cell factor (SCF), FLT3 ligand (FL), thrombopoietin (TPO), and IL-6/soluble IL-6 receptor (sIL-6R) was found to expand HSCs most efficiently, with a 4.2-fold increase in severe combined immunodeficient (SCID)-repopulating cells (SRC) [4]. Several patients have received the transplantation with cytokine-expanded CB HSCs, and these cells were transplanted without serious toxicities [5, 6]. However, although increased numbers of infused CB HSCs were shown to correlate with good outcomes, cytokine-expanded CB HSCs did not shorten the nadir period after transplantation, indicating the

Correspondence: Hirokazu Tanaka, M.D., Ph.D., Department of Hematology and Oncology, Osaka University Graduate School of Medicine, C9, 2-2, Yamada-oka, Suita, Osaka 565-0871, Japan. Telephone: 81-6-6879-3871; Fax: 81-6-6879-3879; e-mail: htanaka@fbri.org Received September 6, 2005; accepted for publication July 14, 2006. 1066-5099/2006/$20.00/0
doi: 10.1634/stemcells.2006-0434

limited usefulness of cytokines for ex vivo expansion of CB HSCs. Thus, further improvement in ex vivo expansion procedures is necessary to prepare more efficient HSCs.

During the last few years, several molecules that can contribute to HSC self-renewal have been identified and characterized. These include external signaling molecules such as Wnt [7–10], bone morphogenic protein (BMP) [11], Sonic hedgehog (SHH) [12], and Notch ligands [13–15]. Furthermore, endogenous transcriptional modulators such as HOXB4 and Bmi-1 have been shown to be important for HSC self-renewal [16–18]. Among these, HOXB4 is of particular interest because it promotes prominent expansion of HSCs without causing leukemia. When HOXB4 was introduced into murine or human HSCs by gene transfer or protein delivery, these HSCs could be expanded without losing their normal potentials for differentiation into all lineages and for long-term repopulation, with a few exceptions [16, 19–22]. In addition to HOXB4, other HOX homeobox transcription factors play important roles in the proliferation and differentiation of hematopoietic cells [23, 24]. For example, HOXA9 regulates HSCs by mediating the expression of a variety of gene families [25, 26]. HOXA5/A10 and HOXB6 induce differentiation toward the myelomonocytic or erythroid lineage, respectively [27–30]. Furthermore, other HOX transcription factors, especially paralogous groups from A, B, and C, are expressed in normal hematopoietic cells; however, their physiological functions have not been elucidated.

HOX proteins have been demonstrated to interact with non-HOX homeobox family proteins (i.e., PBX and MEIS) at the DNA sequence 5′-TGATNNAT(G/A)(G/T)-3′ in the regulatory region of target genes [31, 32]. These protein complexes regulate target gene expression both positively and negatively, dependent on binding to coactivators or corepressors such as CBP/p300, histone deacetylases, or NcoR/SMRT [33–36]. For a subset of HOX proteins, the formation of a HOX-PBX-DNA ternary complex is mediated through both the HOX homeodomain and a short, conserved YPWM motif located just upstream of the HOX homeodomain [37, 38]. The interaction between the YPWM motif of HOX and the third α-helix in the homeodomain of PBX1 is thought to modify HOX-PBX1 DNA-binding affinity and transcriptional activity [39–41]. In addition, it was reported that PBX1 expressed in HSCs is a negative regulator of HOXB4-mediated self-renewal of HSCs [42]. Consistent with this report, a very recent study demonstrated that although DNA-binding activities are necessary for HOXB4 to expand HSCs ex vivo, the interaction with PBX1 is dispensable for this function [43].

In an attempt to expand potent CB HSCs with high efficiency, we synthesized a peptide containing the YPWM motif from HOX, which was predicted to modify HOX function by inhibiting binding between the YPWM motif in endogenous HOX and the PBX1 homeodomain. Here we show that this decoy HOX (decHOX) peptide augments the cytokine-dependent ex vivo expansion of CD34-positive hematopoietic stem/progenitor cells ($CD34^+$ hHSCs/HPCs), and these cells have the ability to reconstitute hematopoiesis more effectively and rapidly in mice that received transplants.

Materials and Methods

Peptide Synthesis

Peptides were synthesized at Greiner Bio-One (Tokyo, Japan, http://www.gbo.com/en) with purities of more than 95%. Synthetic peptides were lyophilized and stored at −20°C until use.

Reagents and Antibodies

Recombinant human SCF, TPO, IL-6, and sIL-6R were provided by Kirin Brewery (Tokyo, Japan, http://www.kirin.co.jp/english/). Recombinant human FL was purchased from R&D Systems Inc. (Minneapolis, http://www.rndsystems.com). Anti-asialo-GM1 antibody (Ab) was purchased from Wako Chemical (Osaka, Japan, http://www.wako-chem.co.jp/english). Antibodies (Abs) against HOXB4 (N-18) and PBX1 (P-20) were purchased from Santa Cruz Biotechnology Inc. (Santa Cruz, CA, http://www.scbt.com).

Plasmids

The expression vectors for HOXB4 and PBX1 were kindly provided by Dr. R. K. Humphries (British Columbia Cancer Agency, Vancouver, BC, Canada) and Dr. M. Featherstone (McGill University, Montreal, QC, Canada), respectively.

Preparation of Glutathione *S*-Transferase Fusion Proteins

Mutants of PBX1 were generated by polymerase chain reaction (PCR) and subcloned into pGEX-5X-1 (GE Healthcare Bio-science Corp., Piscataway, NJ, http://www.gehealthcare.com). Glutathione *S*-transferase (GST)-PBX1 fusion proteins were produced in *Escherichia coli* and purified as described previously [44].

In Vitro Binding Assays Using the BIAcore System

To assess in vitro binding between decHOX and PBX1, we used the BIAcore system (Biacore AB, Uppsala, Sweden, http://www.biacore.com/lifesciences/index.html). The details of this system are described elsewhere [45]. Briefly, we immobilized decHOX on the surface of CM5 sensor chips. Solution containing each GST-PBX1 fusion protein was injected over the sensor chips. Binding kinetics were monitored by changes in the weight of sensor chips and evaluated as arbitrary resonance units (RUs).

Mice

Nonobese diabetic/Shi-severe combined immunodeficient (NOD/SCID) mice, which lack mature lymphocytes and circulating complement proteins and have defective macrophages, were obtained from Jackson Laboratory (Bar Harbor, ME, http://www.jax.org). The mice were kept in microisolator cages on laminar flow racks in a clean experiment room and fed an irradiated, sterile diet and autoclaved, acidified water. Animal care was in accordance with institutional guidelines.

Cell Preparation

Human umbilical CB was obtained from normal, full-term deliveries upon obtaining informed consent. After sedimentation of the red blood cells with 6% hydroxyethyl starch (HES), mononuclear cells (MNCs) were separated by Ficoll-Hypaque density gradient centrifugation. $CD34^+$ cells were purified from MNCs using a MACS Direct CD34 Progenitor Cell Isolation Kit

(Miltenyi Biotec, Bergisch Gladbach, Germany, http://www.miltenyibiotec.com). After purification, over 95% of the separated cells were confirmed to be $CD34^+$ by flow cytometric analysis (data not shown). Each experiment was performed with cord blood $CD34^+$ cells derived from the same sample.

Suspension Cultures

Purified $CD34^+$ cells were seeded at a cell density of $1–2 \times 10^4$ cells per milliliter in 24-well tissue plates (Falcon, Becton, Dickinson and Company, Franklin Lakes, NJ, http://www.bd.com) with QBSF-60 serum-free medium (Quality Biological, Inc., Gaithersburg, MD, http://www.qualitybiological.com) containing SCF (100 ng/ml), FL (100 ng/ml), TPO (10 ng/ml), IL-6 (100 ng/ml), and sIL-6R (100 ng/ml). Cells were cultured in humidified air with 5% CO_2 at 37°C.

Protein Delivery

Synthetic peptides were delivered into 293T and CB $CD34^+$ cells using the Profect Protein Delivery System (Targeting Systems, Santee, CA, http://www.targetingsystems.com) according to the manufacturer's instructions.

Colony Assays

Cells were seeded into methylcellulose medium (MethoCult GF H4434V; Stem Cell Technologies, Vancouver, BC, Canada, http://www.stemcell.com) at a density of 2.5×10^2 cells per 35-mm dish and were cultured with 5% CO_2 at 37°C. All cultures were performed in triplicate, and the numbers of colonies were counted after 10 days.

Reconstitution Assays Using NOD/SCID Mice

Transplantation assays using NOD/SCID mice were performed according to procedures described previously [4] with some modifications. Briefly, 6–8-week-old NOD/SCID mice were total-body irradiated (TBI) with a dose of 2.4 Gy (60 Co) and then transplanted with the whole of peptide-treated cells or 2×10^4 freshly isolated $CD34^+$ cells through the tail vein. Because natural killer cell activity is retained in NOD/Shi-scid mice, the recipients were injected i.p. with 400 μl of phosphate-buffered saline containing 20 μl of anti-asialo-GM1 Ab immediately before cell transplantation. Identical treatments were performed on days 7 and 14. The proportion of reconstituted human cells in peripheral blood (PB) or bone marrow (BM) was assessed by flow cytometry with the anti-human CD45 Ab. For secondary transplantations, bone marrow cells were obtained from tibiae and femurs of the first mice that received transplants 12 weeks after transplantation, and 0.5×10^7 total bone marrow chimeric cells were injected into secondary NOD/SCID recipients subjected to immunosuppressive treatment before and after transplantation as described above ($n = 5$). Six weeks after transplantation, the presence of transplanted human cells in recipient BM was confirmed by flow cytometry as described above.

Limiting Dilution Analysis

The frequencies of human HSCs that were capable of repopulating in NOD/SCID mice in freshly isolated CB $CD34^+$ cells and peptide-treated cells were quantified by a limiting dilution analysis as described previously [46–48]. In this analysis, to avoid graft rejection, the recipients were treated with TBI in combination with anti-asialo-GM1 Ab immediately before and after transplantation (days 7, 14, 21, and 28). Data from several limiting dilution experiments were pooled and analyzed by applying Poisson statistics to the single-hit model. Frequencies were calculated using the maximum likelihood estimator.

Luciferase Assays

The details of the −1,137-c-*myc*-Luc vector, containing a 1,653-base pair (bp) fragment of the c-*myc* promoter (–1,137 to +516), were described previously [49]. To construct 3 × HB4(–316)-Luc and 3 × HB4(–72)-Luc, three tandem repeats of HOXB4-responsive elements at the indicated positions in the insulin-like growth factor-binding protein (IGFBP)-1 promoter were subcloned into pGL3 basic-TK-Luc. The sequences of the HOXB4-responsive elements were as follows: HB4(–316), 5′-CTTGTGTCAATTAAAGA and HB4(–72), 5′-GCGCTGCCCAATCATTAA. Luciferase assays were performed with a Dual-Luciferase Reporter System (Promega, Madison, WI, http://www.promega.com) as previously described [50]. Briefly, 293T cells (2×10^5 cells) were seeded in a 60-mm dish and cultured for 24 hours. Using the calcium phosphate coprecipitation method, cells were transfected with 6 μg of pcDNA3-HOXB4 alone or in combination with 6 μg of pCS2-PBX1a, along with 2 μg of reporter gene and 10 ng of pRL-CMV, a *Renilla* luciferase expression vector. After 12 hours, cells were washed, serum-starved for 24 hours, and subjected to luciferase assays. In some experiments, various doses of synthetic peptides were delivered into 293T cells 24 hours prior to luciferase assays.

Electrophoretic Mobility Shift Assay

Electrophoretic mobility shift assay (EMSA) was performed as previously described [51]. The double-stranded oligonucleotide HB4(–316) (described above) was used as a probe or competitor.

Semiquantitative Reverse Transcription PCR Analysis

Total RNA was isolated from 5×10^4 cells using a Concert Micro-to-Midi Total RNA Purification System (Invitrogen, Carlsbad, CA, http://www.invitrogen.com). Reverse transcription PCR (RT-PCR) was performed using a SuperScript One-Step RT-PCR system (Invitrogen) according to the manufacturer's instructions with forward/reverse primer sets as follows: c-myc, 5′-CTT CTG CTG GAG GCC ACA GCA AAC CTC CTC and 5′-CCA ACT CCG GGA TCT GGT CAC GCA GGG; $p21^{waf1/cip1}$, 5′-ACA GCA GAG GAA GAC CAT GT and 5′-GGT ATG TAC ATG AGG AGC TG; and β-actin, 5′-GGC GGC AAC ACC ATG TAC CCT and 5′-AGG GGC CGG ACT CGT CAT ACT.

Chromatin Immunoprecipitation Assays

Chromatin immunoprecipitation (ChIP) assays were performed with a ChIP Assay Kit (Upstate, Charlottesville, VA, http://www.upstate.com). Briefly, after transfection with various expression vectors, 293T cells were fixed with 1% formaldehyde. After isolation of nuclear extract, the chromatin was sonicated. Then, protein-DNA complexes were immunoprecipitated with 2 μg of anti-PBX1, anti-HOXB4, or anti-actin Ab. Immunoprecipitated DNA was eluted and subjected to PCR analysis with the following primer pair to amplify 420 bp of the human IGFBP-1 promoter (M59316): forward primer, 5′-GGC ATT

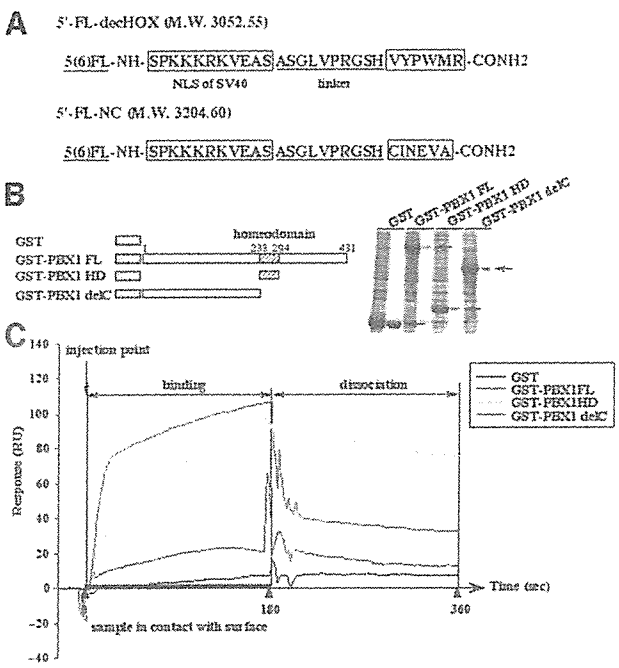

Figure 1. Binding of decHOX to GST-PBX1. **(A):** The structures of the 5′-FL synthetic peptides 5′-FL-decHOX and 5′-FL-NC are indicated. **(B):** GST-PBX1 fusion proteins expressed in *E. coli* were purified by glutathione-Sepharose 4B beads, and their qualities and quantities were confirmed by Coomassie staining. **(C):** In vitro binding of GST-PBX1 to decHOX evaluated by the BIAcore system, with decHOX attached to the sensor chip. To examine the kinetics of the binding and dissociation, various GST-PBX1 proteins were injected onto the sensor chip for 180 seconds and then washed with HEPES-buffered saline for 180 seconds. Abbreviations: decHOX, decoy HOX; delC, C-terminal deletion; FL, fluorescein; GST, glutathione *S*-transferase; HD, homeobox domain; M.W., molecular weight; NC, negative control; NH NLS, nuclear localization signal; RU, resonance unit.

GTT TTC TGC GTT TGA GAA CTG CTG; reverse primer, 5′-CTG GAC ACA GCG CGC ACC TTA TAA AGG GCA. After electrophoresis, PCR products were visualized with ethidium bromide staining.

Statistical Analysis

Data are presented as mean ± SEM or mean ± SD. The statistical significance of the data was determined by the Mann-Whitney *U* test or Student's *t* test. The significance level was set at .05.

Results

The Synthetic Peptide decHOX Binds Directly to the Homeodomain of PBX1

In this study, we attempted to expand CB CD34$^+$ hHSC/HPCs by modifying the function of HOX family proteins. For this purpose, we designed and synthesized a peptide designated decHOX, which was expected to inhibit the interaction between HOX and PBX1. decHOX contains the YPWM motif of HOX, used for its cooperative interaction with PBX1 [36, 37], and the nuclear localization signal (NLS) of the SV40 large T antigen (Fig. 1A) [52]. The negative control (NC) peptide contains the unrelated amino acid sequence CINEVA. To evaluate the efficiency of peptide delivery into CB CD34$^+$ hHSC/HPCs and the subsequent kinetics, FL protein was conjugated to the N termini of both peptides.

First, we examined in vitro binding between decHOX and several GST-PBX1 fusion proteins using the BIAcore system. In this system, the analyte protein is injected onto the sensor chip, the surface of which is covered by the immobilized partner ligand. Binding of the ligand to the analyte is monitored by an increase in arbitrary RUs. Prior to this analysis, we purified several GST-PBX1 fusion proteins (Fig. 1B, left panel) and confirmed their qualities and quantities by Coomassie Brilliant Blue staining (Fig. 1B, right panel). Injection of either GST-full-length PBX1 protein (GST-PBX1 FL) or GST-PBX1 homeobox domain (HD) protein (GST-PBX1 HD) over the decHOX surface resulted in a significant increase in RUs with a lapse of 3 minutes for the binding reaction (Fig. 1C), and these signals increased in a dose-dependent manner (data not shown). In contrast, GST alone and GST-PBX1 delC (lacking the HD) did not bind appreciably to decHOX. After the binding reaction, we injected HEPES-buffered saline for 180 seconds. During this dissociation reaction, GST-PBX1 HD bound to decHOX more stably than GST-PBX1 FL (Fig. 1C). These results suggest that GST-PBX1 FL and GST-PBX1 HD bind to decHOX, probably through HD.

decHOX Can Modulate the Transcriptional Activity of HOX-PBX

To assess the effects of decHOX on HOX-PBX-mediated gene expression, we performed luciferase assays with three types of reporter genes for HOXB4, one containing the c-*myc* promoter (–1,137-c-*myc*-Luc) and the other two containing IGFBP-1 promoters (3 × HB4[–316]-Luc and 3 × HB4[–72]-Luc) as responsive elements, as described previously [49, 53]. Although HOXB4 activated –1,137-c-*myc*-Luc 5.2-fold in 293T cells, PBX1 suppressed this induction (Fig. 2B). However, this inhibitory effect of PBX1 was decreased in a dose-dependent manner by pretreatment with decHOX. Similar responses were observed in assays using 3 × HB4(–316)-Luc and 3 × HB4(–72)-Luc (Fig. 2B). These results indicate that decHOX can enhance the activity of HOXB4 that is suppressed by PBX1.

In a previous study using EMSA, mutant HOX proteins that cannot bind to PBX1 were shown to have defects in DNA-binding activities [39–41]. In contrast, it was reported that the interaction with PBX1 is not necessary for HOXB4 to induce HSC self-renewal [43]. Because decHOX was designed to inhibit the interaction between HOX and PBX1, we evaluated the effect of decHOX on the DNA-binding activity of HOXB4-PBX1 using EMSA. For this purpose, we transfected 293T cells with wild-type (WT) HOXB4 or mutant HOXB4 harboring a WM→AA mutation in the YPWM motif (designated HOXB4 AA; Fig. 2C). Protein(s) in nuclear extracts from 293T cells transfected with PBX1 and HOXB4 WT bound to the HB4(–316) probe (Fig. 2C, lane 2). This band was abolished by WT DNA competitor (Fig. 2C, lane 3) but not by mutant (mt) competitor (Fig. 2C, lane 4), implying that it contains the HOXB4 WT-PBX1 complex. In contrast, proteins in the nuclear extract from HOXB4 AA-transfected cells scarcely bound to the probe, indicating the importance of the YPWM motif for the DNA-binding activity of HOXB4-PBX1 (Fig. 2C, lane 5). Also, pretreatment with decHOX inhibited DNA binding of the HOXB4 WT-PBX1 complex in a dose-

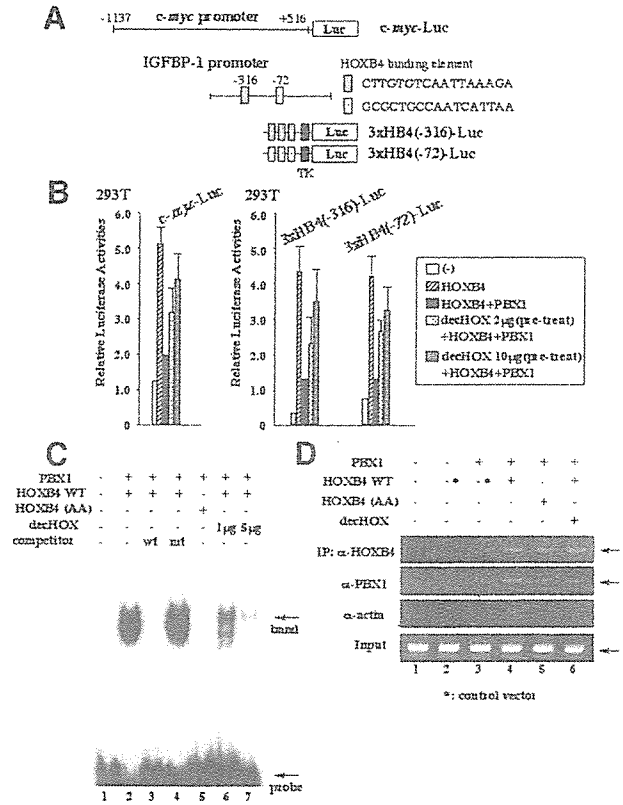

Figure 2. Effects of decHOX on DNA-binding and transcriptional activities of the HOX/PBX complex. **(A):** To construct –1,137-c-*myc*-Luc, a 1,653-base pair fragment of the c-*myc* promoter (–1137 to +516) was subcloned into the plasmid pSP72-Luciferase [47]. To generate 3 × HB4(–316)-Luc and 3 × HB4(–72)-Luc, three tandem repeats of HOXB4-responsive elements in the IGFBP-1 promoter at the indicated locations were subcloned into TK-pGL3 basic-Luc at just upstream of the murine minimal TK promoter linked to the firefly luciferase gene, and their sequences were as indicated. **(B):** 293T cells (2×10^5 cells) seeded in a 60-mm dish were transfected with 6 μg of pcDNA3-HOXB4 alone or in combination with 6 μg of pCS2-PBX1a along with 2 μg of reporter gene and 10 ng of pRL-CMV. After 12 hours, cells were washed, serum-starved for 24 hours, and subjected to luciferase assays using a Dual Luciferase Reporter Assay System. In some experiments, various doses of synthetic peptides were delivered into 293T cells 24 hours prior to luciferase assays. Results are shown as mean ± SD of triplicate cultures. **(C):** 293T cells were transfected with PBX1 together with HOXB4 WT or HOXB4 AA. After 36 hours, nuclear extract was isolated and subjected to electrophoretic mobility shift assay (EMSA) with probes of 3 × HB4(–316). In competition assays, a 200-fold excess of unlabeled wt or mt competitor oligonucleotide was added to the binding mixture. In some experiments, various doses of synthetic peptides were delivered into 293T cells 24 hours prior to EMSA. **(D):** 293T cells transfected with the indicated expression vectors were fixed with 1% formaldehyde. After the isolation of the nuclear extract, chromatin was sonicated. Then, protein-DNA-binding complexes were immunoprecipitated with the 2 μg of the indicated antibodies. Immunoprecipitated DNA was subjected to polymerase chain reaction (PCR) analysis with a primer pair that amplifies 420 base pairs of the human IGFBP-1 promoter. PCR products were electrophoresed onto the agarose gel and visualized with ethidium bromide staining. Abbreviations: decHOX, decoy HOX; IGFBP-1, insulin-like growth factor-binding protein; IP, immunoprecipitation; mt, mutant; WT, wild type.

dependent manner (Fig. 2C, Lanes 6 and 7). These results suggest that decHOX inhibits the interaction between HOXB4 and PBX1 in the ex vivo EMSA binding experiment, thereby suppressing the DNA-binding activity of the HOXB4 WT-PBX1 complex. However, in ChIP assays, which reflect the in vivo DNA-binding state of transcription factors more precisely than EMSA, the HOXB4 AA-PBX1 complex bound to the endogenous IGFBP-1 promoter as efficiently as the HOXB4 WT-PBX1 complex (Fig. 2D, top and second panels, lane 4 vs. lane 5). Also, decHOX barely influenced the DNA-binding activity of the HOXB4 WT-PBX1 complex (Fig. 2D, top and second panels, lane 4 vs. lane 6). Furthermore, we obtained similar results from ChIP assays using two additional primer sets that amplify different sites in the IGFBP-1 promoter (data not shown). From these results, we speculated that HOXB4 is capable of binding to DNA regardless of its interaction with PBX1. However, since we found that PBX1 bound to target DNA in the presence of HOXB4 AA, it is also possible that the YPWM is not required for the interaction between HOXB4 and PBX1. Because the latter speculation is inconsistent with several previous reports indicating the essential role of the YPWM motif in the interaction between HOXB4 and PBX1 [37, 38], further studies using several endogenous promoter sequences will be required to draw a definite conclusion.

decHOX Is Efficiently Delivered into CB CD34$^+$ and Colocalizes with PBX1

Next, we introduced 5′-FL-decHOX into CB CD34$^+$ hHSC/HPCs and analyzed the efficiency of delivery by examining fluorescein intensity with flow cytometry. CD34$^+$ hHSC/HPCs were isolated from CB using AutoMACS and cultured in QBSF-60 serum-free medium containing SCF, FL, TPO, IL-6, and sIL-6R. After culturing for 24 hours, FL-decHOX or FL-NC was delivered into CD34$^+$ cells using the Profect Protein Delivery System. Immediately after delivery (day 0; total culture day 2), 76.2% of CB CD34$^+$ cells were fluorescein-positive (Fig. 3A). Fluorescein intensity decreased with time in culture and was scarcely detectable at day 7. This result suggested that the direct influence of decHOX on CD34$^+$ hHSC/HPCs is limited to 7 days.

Next, we examined the subcellular localizations of PBX1, decHOX, and the NC peptide in hHSC/HPCs using fluorescent microscopy. Forty-eight hours after peptide delivery, both peptides were predominantly detected in the nucleus because of the respective nuclear localization signals. In NC-delivered cells, PBX1 was mainly localized in the cytosol (Fig. 3B, upper panel). On the other hand, in decHOX-delivered cells, PBX1 colocalized with decHOX in the nucleus (Fig. 3B, lower panel). These results suggested that decHOX could interact with PBX1 and colocalized with PBX1 in the nucleus.

decHOX Can Modulate HOX/PBX-Mediated Gene Expression in CB hHSC/HPCs

PBX1 is known to modulate the function of HOX proteins both positively and negatively [30, 32, 33]. For example, HOXB4 induces the expression of c-*myc* in HSCs, and this effect is suppressed by PBX1. On the other hand, HOXA10-mediated expression of $p21^{waf1/cip1}$ is enhanced by PBX1 in myelomonocytic progenitors [28]. To assess the effects of decHOX on the function of HOX proteins in CB cells, we examined the expression of these two target genes. First, to characterize CD34$^+$CD38$^+$ and CD34$^+$CD38$^-$ cells after the ex vivo expansion, we sorted these cells after 9 days in culture and

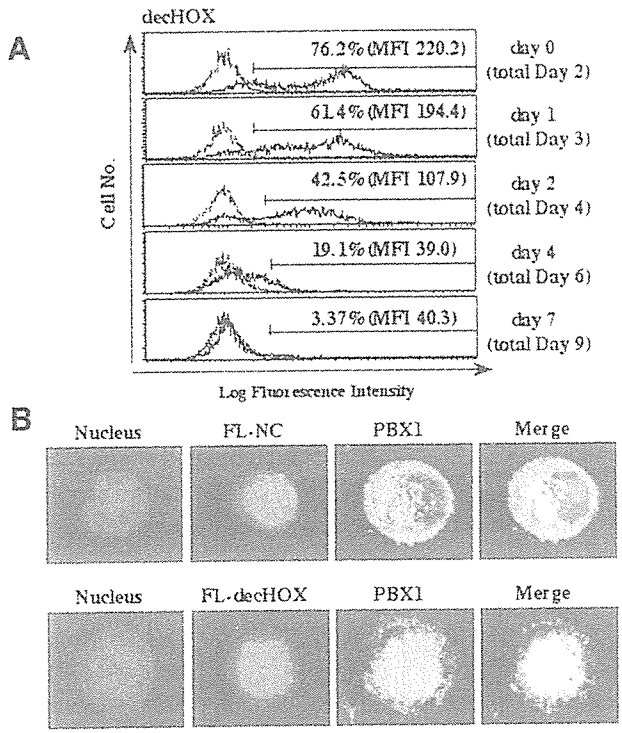

Figure 3. Expression and intracellular localization of decHOX in hHSC/HPCs. **(A):** FL-decHOX was transferred into $CD34^+$ cells by the Profect Protein Delivery System, and fluorescence intensity was assessed by flow cytometry at the indicated times. **(B):** Cytospin preparations of the FL-NC (upper panel)- or FL-decHOX (lower panel)-delivered $CD34^+$ cells were fixed, permeabilized, and incubated with a rabbit anti-human PBX1 antibody (Ab) for 1 hour and then with the anti-rabbit IgG Ab AlexaFluor 546. Cells were rinsed with phosphate-buffered saline containing Hoechst 33342. The stained cells were observed under a confocal laser microscope. Abbreviations: decHOX, decoy HOX; MFI, mean fluorescence intensity; NC, negative control.

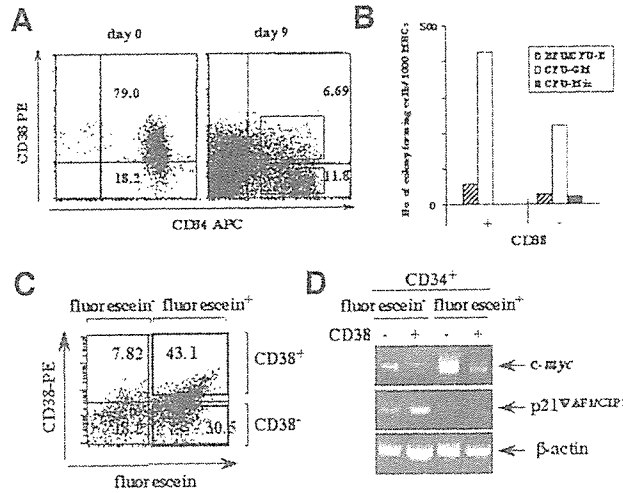

Figure 4. Effects of decoy HOX (decHOX) on target gene expression in hHSC/HPCs. Cord blood (CB) $CD34^+$ cells were cultured in QBSF-60 serum-free medium containing cytokines (stem cell factor, 100 ng/ml; fluorescein [FL], 100 ng/ml; TPO, 10 ng/ml; IL-6, 100 ng/ml; and sIL-6R, 100 ng/ml) for 9 days. **(A):** Before and after culturing, the expression of CD34 and CD38 were examined by flow cytometry. **(B):** After culturing, $CD34^+CD38^-$ and $CD34^+CD38^+$ cells were sorted and subjected to colony assays. **(C):** CB $CD34^+$ cells were treated with FL-decHOX for 48 hours, and then CD38 and fluorescein expression was examined by flow cytometry. **(D):** Cells from each fraction were sorted and subjected to RT-PCR analysis. Abbreviations: APC, allophycocyanin; CFU-GM, colony-forming unit-granulocyte/monocyte precursor; CFU-mix, mixed hematopoietic colony-forming unit.

performed methylcellulose colony assays (Fig. 4A). It was reported that $CD34^+CD38^-$ cells can develop from $CD34^+CD38^+$ cells through the loss of CD38 expression during culturing with cytokines [54]. We found that the primitive colony, mixed hematopoietic colony-forming unit (CFU-Mix) was formed from $CD34^+CD38^-$ cells but not from $CD34^+CD38^+$ cells. Therefore, we supposed that $CD34^+CD38^-$ cells were more primitive than the $CD34^+CD38^+$ cells that developed after ex vivo culturing. Next, we treated CB $CD34^+$ cells with 5′-FL-decHOX, cultured for 48 hours, and subjected them to flow cytometric analysis. At that point, 43.1% of the cultured cells were $fluorescein^+CD38^+$, 30.5% were $fluorescein^+CD38^-$, 7.82% were $fluorescein^-CD38^+$, and 18.2% were $fluorescein^-CD38^-$ (Fig. 4C). Then, we sorted the cells from each fraction and subjected them to semiquantitative RT-PCR analysis. In the $CD34^+CD38^-$ immature cell fraction, c-*myc* expression was increased in the decHOX-delivered $fluorescein^+$ fraction compared with the $fluorescein^-$ control fraction (Fig. 4D, top panel, lane 1 vs. lane 3). Conversely, in the $CD34^+CD38^+$ mature fraction, the expression of $p21^{waf1/cip1}$ was decreased in the $fluorescein^+$ fraction compared with the $fluorescein^-$ fraction (Fig. 4D, middle panel, lane 2 vs. lane 4). Together, these results suggest that decHOX binds to PBX1 as a HOX decoy and cancels both the positive and negative effects of PBX1 on HOX proteins in $CD34^+$ hHSC/HPCs.

decHOX Enhances Cytokine-Dependent Ex Vivo Expansion of CB hHSC/HPCs

Next, we examined effects of decHOX on the growth and differentiation of CB $CD34^+$ hHSC/HPCs. As shown in Figure 5, purified $CD34^+$ cells were exposed to 5′-FL-decHOX or 5′-FL-NC for 24 hours. Then, 1×10^4 $fluorescein^+$ cells were sorted and cultured in QBSF-60 serum-free medium containing SCF, FL, TPO, IL-6, and sIL-6R for 7 days, during which, medium dilution was performed as indicated. After these cultures, no apparent difference was observed between the total number of viable decHOX-treated and NC-treated cells (Fig. 6A). However, the proportion of $CD34^+$ cells was significantly higher in decHOX-treated cells than in NC-treated cells (decHOX, 33.2%; NC, 17.9%) (Fig. 6B). Similar results were obtained from five independent experiments (data not shown). Accordingly, the fold expansion of $CD34^+$ cells was higher in decHOX-delivered cells than in NC-delivered cells (decHOX, 32.5 ± 8.71-fold; NC, 17.2 ± 6.25-fold [$n = 6$] [$p < .05$]) (Fig. 6A). Furthermore, cultures treated with decHOX retained immature cells with $CD34^+CD38^-$ or $CD45^+HLA\text{-}DR^-$ phenotype more effectively than NC-treated cells (percentage $CD34^+CD38^-$ cells: decHOX, $24.2\% \pm 6.67\%$; NC, $14.8\% \pm 6.17\%$ [$n = 3$] [$p < .05$]; percentage $CD45^+HLA\text{-}DR^-$ cells: decHOX, $37.2\% \pm 6.98\%$; NC, $18.8\% \pm 7.44\%$ [$n = 3$] [$p < .05$]) (representative results from one experiment are shown in Fig. 6B). To characterize the ex vivo expanded cells, we ana-

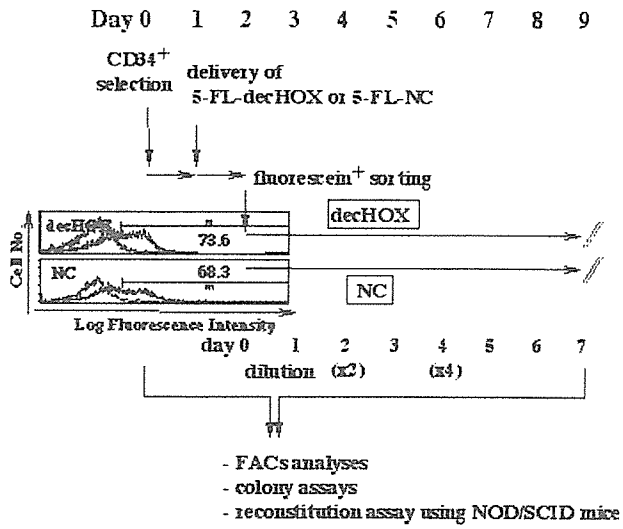

Figure 5. Experimental design. CD34$^+$ hematopoietic stem/progenitor cells were isolated from cord blood and cultured in serum-free medium containing cytokines. FL-decHOX or FL-NC was then delivered into CD34$^+$ cells. Twenty-four hours after peptide delivery, approximately 70% of cultured cells were fluorescein-positive. Fluorescein-positive cells were sorted and cultured for 7 days. Medium dilutions were performed as indicated. Cultured cells were then subjected to FACS analyses, colony assays, and reconstitution assays using NOD/SCID mice. Abbreviations: decHOX, decoy HOX; FACS, fluorescence-activated cell sorting; FL, fluorescein; NC, negative control.

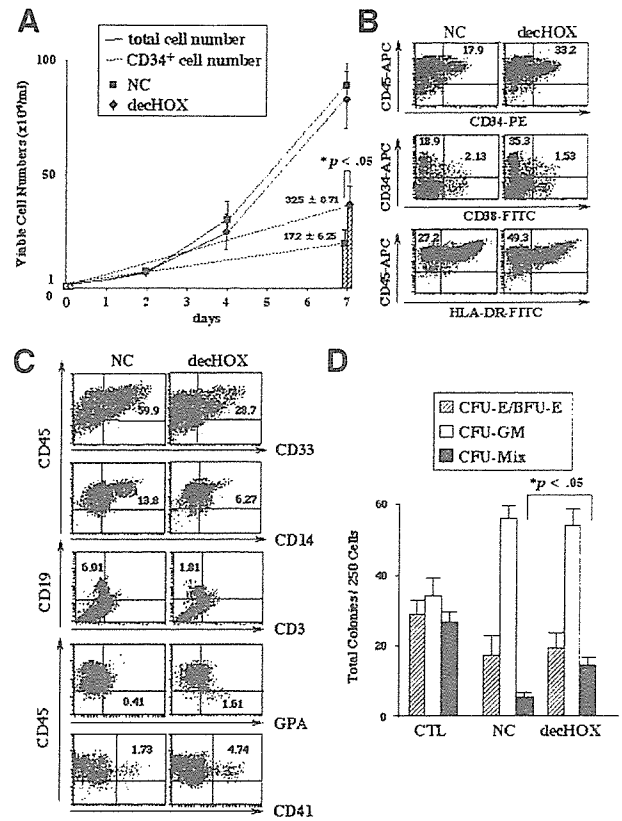

Figure 6. Effects of decHOX on biological properties and functions of hHSC/HPCs cultured with cytokines. After treatment with fluorescein (FL)-decHOX or FL-NC, fluorescein-positive cells were sorted and cultured for 7 days. **(A):** The total number of viable cells and their surface phenotypes were examined. Results are shown as mean ± SD (n = 6). **(B, C):** Representative fluorescence-activated cell sorting data from one experiment are shown. **(D):** Cultured cells were subjected to methylcellulose colony assays using freshly isolated cells as a control. All cultures were done in triplicate and scored after 10 days. Results are shown as mean ± SD (n = 4). Abbreviations: BFU-E, burst-forming unit-erythroid precursor; CFU-E, colony-forming unit-erythrocyte precursor; CFU-GM, colony-forming unit-granulocyte/monocyte precursor; CFU-Mix, mixed hematopoietic colony-forming unit; CTL, control; decHOX, decoy HOX; FITC, fluorescein isothiocyanate; HLA, human leukocyte antigen; NC, negative control; PE, phycoerythrin.

lyzed the expression of lineage markers on these cells (Fig. 6C). Fluorescence-activated cell sorting analyses after 7 days in culture indicated that both NC- and decHOX-treated cells contained not only immature cells but also mature cells expressing lineage markers such as CD33 (myeloid), CD14 (monocytic), CD19 (B lymphoid), GPA (erythroid), and CD41 (megakaryocytic). Except for GPA and CD41 expression, the expression of these markers was notably lower in decHOX-delivered cells than in NC-delivered cells. Next, we analyzed the effects of decHOX on colony-forming activities of CB CD34$^+$ hHSC/HPCs. As shown in Figure 6D, both decHOX- and NC-delivered cells, which contain approximately 33% and 18% of CD34$^+$ cells, respectively (Fig. 6B), generated all types of colonies, and the numbers of colony-forming unit-erythrocyte precursor/burst-forming unit-erythroid precursor and colony-forming unit-granulocyte/monocyte precursor colonies were nearly the same in both cultures. However, decHOX more effectively yielded CFU-Mix primitive colonies than NC (CFU-Mix colonies per 250 cultured cells: decHOX, 15.3 ± 2.1; NC, 7.5 ± 0.8 [n = 6] [$p < .05$]). Together, these results suggest that although both immature progenitors and mature cells were amplified during culturing, decHOX selectively expands immature progenitors.

decHOX-Treated hHSC/HPCs Reconstitute Hematopoiesis Rapidly and Efficiently in NOD/SCID Mice

Next, we assessed the effects of decHOX on engrafting abilities of CB CD34$^+$ hHSC/HPCs by xenotransplantation into NOD/SCID mice. For this purpose, 2 × 10^4 CB CD34$^+$ cells were treated with decHOX or NC and cultured in QBSF-60 containing cytokines for 7 days. Then, total cultured cells were transplanted into NOD/SCID mice that were treated with 2.4 Gy of TBI and i.p. injection of anti-asialo-GM1 Ab immediately before and after transplantation (days 7 and 14) (each group, n = 9). Also, 2 × 10^4 freshly isolated CB CD34$^+$ cells derived from the same sample as the expanded cells were transplanted as a control (CTL). CTL cells are expected to contribute to hematopoiesis in approximately 10% of BM cells after 4 weeks under our experimental conditions using NOD/SCID mice. When decHOX-treated cells were transplanted, human CD45$^+$ (hCD45$^+$) cells constituted 9.17% of the BM cells 4 weeks after transplantation, whereas NC-treated cells yielded only 4.28% hCD45$^+$ cells (Fig. 7A). In addition, the proportion of hCD34$^+$ cells in the BM was increased by decHOX (decHOX, 3.05%; NC, 1.22%) (Fig. 7A). We also analyzed the lineage distributions of hCD45$^+$ cells in BM of mice that received transplants of decHOX-treated cells at 4 and 8 weeks after transplantation.

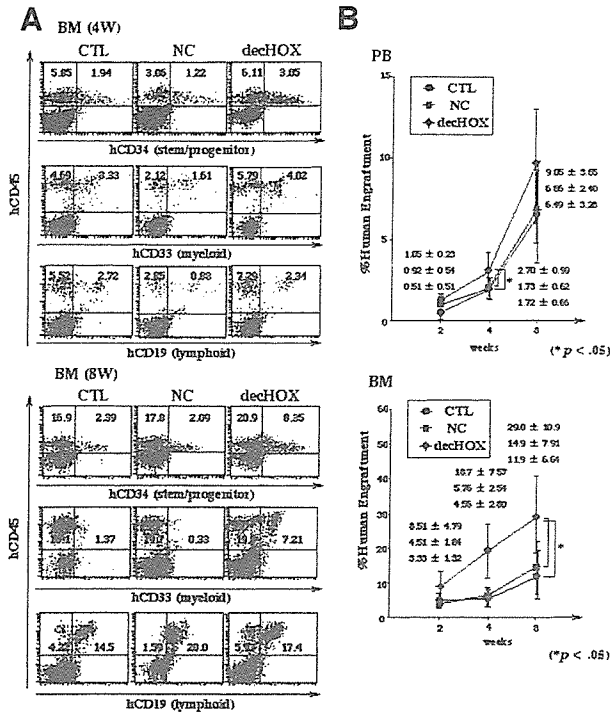

Figure 7. Xenotransplantation into nonobese diabetic/severe combined immunodeficient (NOD/SCID) mice. **(A):** A total of 2×10^4 decHOX- or NC-delivered cells were sorted and subjected to the culture for 7 days. Whole expanded cells or 2×10^4 freshly isolated $CD34^+$ cells were transplanted into 5–6-week-old NOD/SCID mice subjected to immunosuppressive treatment before and after transplantation (each group, n = 9). Four weeks after transplantation, the proportion of engrafted human cells in BM was assessed by flow cytometry with anti-hCD45-PE antibody (Ab). Four weeks and 8 weeks after transplantation, short-term repopulation abilities of the ex vivo-expanded cells were analyzed using BM and PB cells with the indicated Abs. Representative flow cytometry data obtained from BM cells are shown. **(B):** Kinetics of engraftment in PB and BM of NOD/SCID mice are indicated. Results are shown as mean ± SD (each group, n = 9). Abbreviations: BM, bone marrow; CTL, control; decHOX, decoy HOX; NC, negative control; PB, peripheral blood; PE, phycoerythrin; W, weeks.

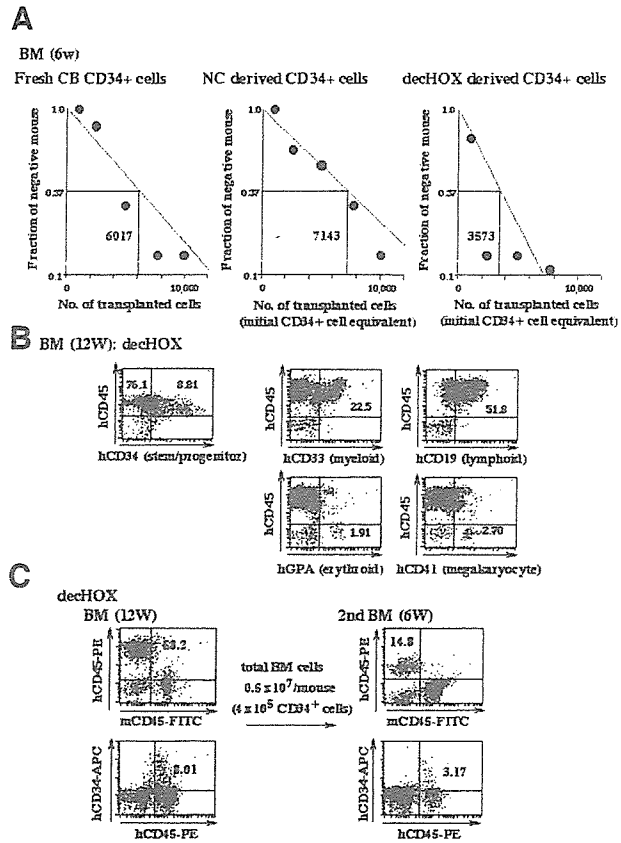

Figure 8. Long-term repopulating abilities in decHOX-delivered cells. **(A):** Frequencies of human HSCs capable of repopulating in nonobese diabetic/severe combined immunodeficient (NOD/SCID) mice in freshly isolated CB $CD34^+$ cells (n = 26), NC-treated cells (n = 29), and decHOX-treated cells (n = 23) were quantified by limiting dilution analyses. **(B):** Twelve weeks after transplantation, the long-term repopulating ability of the decHOX-treated cells was analyzed by flow cytometry using BM from NOD/SCID mouse highly reconstituted with human cells. **(C):** Twelve weeks after transplantation, BM cells were isolated from NOD/SCID mice that received transplants of decHOX-treated cells and injected into secondary recipients (n = 5). Six weeks after transplantation, the proportions of engrafted human cells in BM were assessed by flow cytometry. Representative data are shown. Abbreviations: BM, bone marrow; CB, cord blood; decHOX, decoy HOX; FITC, fluorescein isothiocyanate; hCD, human cluster of differentiation; NC, negative control; PE, phycoerythrin; W, weeks.

As shown in Figure 7A, transplanted decHOX-treated cells not only retained $CD34^+$ cells but also generated $CD33^+$ myeloid cells and $CD19^+$ B cells more effectively than CTL and NC-treated cells.

We also analyzed the kinetics of short-term repopulation in the PB and BM of recipient mice. Two weeks after transplantation, $hCD45^+$ cells were detectable in both BM and PB without significant differences in their frequencies among decHOX, NC, and CTL groups (Fig. 7B). However, at 4 weeks, the proportion of $hCD45^+$ cells in PB was significantly higher in the decHOX group than in the NC and CTL groups (decHOX, 2.70% ± 0.36%; NC, 1.73% ± 0.14%; CTL, 1.72% ± 0.16%) ($p < .05$). This result suggests that decHOX reduces the delay in engraftment associated with CB transplantation (Fig. 7B). Also, the percentage of $hCD45^+$ cells in BM was significantly higher in the decHOX group than in the CTL and NC groups at 8 weeks (decHOX, 29.0% ± 10.9%; CTL, 11.9% ± 6.64%; NC, 14.9% ± 7.91% [$p < .05$]).

Given the possibility that decHOX supports the expansion of long-term repopulating (LTR)-HSCs, we next calculated the expansion rate using a limiting dilution method. To obtain the highest possible levels of human cell engraftment, recipient mice were treated with TBI in combination with anti-asialo GM1 Ab immediately before and after transplantation (days 7, 14, 21, and 28). As shown in Figure 8A, the frequency of LTR-HSCs was calculated to be 1 in 6,017 freshly isolated CB $CD34^+$ cells and 1 in 7,143 NC-treated cells. In contrast, the frequency of LTR-HSCs in decHOX-treated cells was calculated to be 1 in 3,573. Accordingly, the expansion of LTR-HSCs by decHOX was estimated to be 2.0-fold. Furthermore, in BM highly reconstituted with decHOX-treated human cells, we detected considerable proportions of $hCD45^+CD33^+$ cells (22.5%) and $hCD45^+hCD19^+$ cells (51.8%) 12 weeks after transplantation. In addition, $hCD45^+CD34^+$ cells were an estimated 8.81% of total BM cells (Fig. 8B).

To further examine the long-term reconstituting activity of decHOX-treated cells, we performed a secondary transplantation. Twelve weeks after the first transplantation, we isolated BM cells from two mice that received transplants of decHOX-treated cells. A mixture of these cells (58.2% and 8.0% of which were $hCD45^+$ and $hCD34^+$, respectively) was transplanted into five recipients at 4.0×10^5 $hCD34^+$ cells per mouse. An apparent second engraftment was detected in the BM of 2 of 5 mice 6 weeks after the transplantation (representative data are shown in Fig. 8C). At this point, $hCD45^+$ cells were an estimated 14.8% of the total BM cells in the recipient mouse. Furthermore, approximately 20% of $hCD45^+$ cells expressed CD34 (3.17% of total BM cells). Taken together, these results indicate that CB $CD34^+$ hHSCs/HPCs expanded by decHOX reconstitute hematopoiesis more rapidly and efficiently than control cells, and these cells have long-term reconstituting abilities in NOD/SCID mice.

Discussion

HOXB4-deficient mice do not exhibit obvious abnormalities in hematopoiesis except for a minor proliferative defect of HSCs detected by reconstitution assays, suggesting that HOXB4 is dispensable for normal hematopoiesis [55]. It was speculated that HOXB4 functional roles can be replaced by other HOX family members because mice lacking both HOXB4 and HOXB3 had more apparent defects in hematopoiesis than those lacking HOXB4 alone [56]. However, HOXB4 has attracted particular interest during the last few years because its gene transfer induced ~40-fold murine and ~30-fold human HSC expansion ex vivo, suggesting possible clinical applications [16, 21]. Regarding clinical use, there was an initial concern that constitutive expression of HOXB4 in HSCs might cause leukemia. This is because deregulated expression of HOXB8 was found in myeloid leukemia, and HOX family genes are sometimes involved in leukemogenic chromosomal translocations, such as t(7,11)(p15;p15), yielding NUP98-HOXA9 [57, 58]. However, HSCs expanded by HOXB4 treatment reconstituted all hematopoietic lineages in mice that received transplants mice without causing leukemia, indicating that HSCs expressing HOXB4 were regulated by the hematopoietic system [16]. To eliminate any deleterious effects caused by stable HOXB4 gene transfer, Krosl et al. tried to expand murine HSCs by delivering HOXB4 protein [20]. In that study [20], cell membrane-permeable, recombinant TAT-HOXB4 protein was added to the culture medium, inducing a fivefold net expansion of HSCs. Although TAT-HOXB4 was supposed to be delivered with high efficiency, its half-life was estimated to be only 1 hour. In addition, Amsellem et al. tried to expand human CB HSCs using HOXB4 protein [19]. They used HOXB4 protein secreted into the culture supernatant from cocultured MS-5 murine stromal cells, and this approach increased NOD/SCID mouse repopulating cells (SRCs) 2.5-fold. However, the efficiency of protein delivery was not very high, and the coculture system may not be practical for clinical applications. In contrast, our decHOX could be delivered into more than 70% of CB $CD34^+$ hHSC/HPCs and was detected in these cells even after 4 days.

Because similar decoy peptides, such as NFAT and JNK-interacting-protein-1 (JIP-1) decoy peptides were shown to be harmless at the genomic level [59, 60], decHOX may be useful for clinical applications. Furthermore, it is possible to use decHOX in combination with HOX proteins [19, 20] to further augment the activity of HOXB4. However, it should be noted that Brun et al. reported that an excessive amount of HOXB4 introduced by an adenoviral vector system inhibits self-renewal of human CB HSCs and induces myeloid differentiation [22]. Therefore, it is necessary to determine the optimal amount of HOXB4 for enforcing HSC self-renewal.

Recently, DiMartino et al. generated Pbx1-null mice, which died at embryonic day 15 or 16 due to anemia, and reported that PBX1 is required for the maintenance of definitive hematopoiesis and contributes to the mitotic amplifications of progenitor subsets [61]. However, Krosl et al. demonstrated that antisense DNA against PBX1 apparently augmented self-renewal of HSCs overexpressing HOXB4 but was not effective on normal HSCs, suggesting that PBX1 may be a negative regulator of HOXB4-mediated self-renewal of HSCs [42]. In accordance with this result, we found that decHOX could enhance cytokine-mediated self-renewal of HSCs by modifying the function of HOXB4. Furthermore, we found that decHOX restored HOXB4 activity suppressed by PBX1 without affecting DNA-binding activities. The interaction between the YPWM motif in HOX and the homeodomain in PBX1 modifies the DNA-binding affinities of the proteins and their coactivator/corepressor binding-dependent transcriptional activities, and decHOX presumably affects the latter interactions. At present, we know that decHOX can augment HOXB4-dependent transcription of c-*myc*, which we recently identified as a key regulator of HOXB4- and Notch1-mediated HSC self-renewal [49]. However, HOX-PBX complexes regulate a number of genes in HSCs both positively and negatively. Also, PBX1 shows dual (positive and negative) effects on HOX-mediated transcription according to the target genes and/or the cellular context [31, 33, 34]. Thus, further studies to identify the target genes of HOX/PBX1 in HSCs would provide useful information to facilitate decHOX-mediated ex vivo amplification of HSCs.

To date, two groups of investigators have used ex vivo-amplified CB HSCs for transplantation. Shpall et al. [5] isolated $CD34^+$ cells from CB. Forty percent of the isolated cells were expanded in medium containing SCF, G-CSF, and TPO for 10 days, and the remaining 60% were immediately transplanted or stored frozen until transplantation. After high-dose chemotherapy, 37 patients (25 adults, 12 children) received transplants of expanded $CD34^+$ cells and nonexpanded cells with a median dose of 0.99×10^7 nucleated cells per kilogram. The median time to engraftment of neutrophils (neutrophil count $> 500/\mu l$) was 28 days (range, 15–49 days) and that of platelets (platelet $> 20{,}000/\mu l$) was 106 days (range, 38–345 days). The authors of that study concluded that although the ex vivo expansion of CB cells was feasible and safe, expanded HSCs did not improve the time to engraftment in recipients [5]. In a phase I trial, Jaroscak et al. [6] transplanted CB HSCs expanded by PIXY321, FL, and EPO into 28 patients with a median dose of 2.4×10^7 nucleated cells per kilogram. They also concluded that the ex vivo expanded CB HSCs were not effective in shortening the recovery period [6]. In contrast, the present study showed that decHOX can expand short-term as well as long-term SRC, thereby shortening the delay in hematopoietic recovery, suggesting that decHOX may be an effective tool to resolve this problem. Since HSC quiescence is regulated by $p21^{waf1/cip1}$, $p16^{INK4A}$, and

$p18^{INK4C}$ and progenitor quiescence by $p27^{kip2}$ [62–66], a basic study focusing on the expression of cell cycle control molecules in decHOX-transduced cells may clarify the mechanism of decHOX-mediated rapid recovery of hematopoiesis.

In conclusion, in the present study we demonstrated that decHOX can further augment cytokine-mediated ex vivo expansion of CB HSCs and that these expanded HSCs can restore hematopoiesis more rapidly and effectively than freshly prepared CB HSCs. However, it is necessary to further optimize treatment conditions, such as the method and timing of peptide delivery. Also, to enhance the effects of decHOX, it will be useful to explore the combined effects of other signals that can support HSC self-renewal, such as SHH and Wnt. We hope that our decHOX will eventually benefit patients with hematopoietic malignancies.

ACKNOWLEDGMENTS

We are grateful to N. Takada, K. Maruyama, and M. Hirose for technical support and animal care and Y. Ikegami for laboratory management. This work was supported by grants from the Ministry of Health, Labour and Welfare of Japan (number 18790672, to N.T.), Uehara Foundation (to K.Y.), and Hovansha Foundation (to K.Y.).

DISCLOSURES

The authors indicate no potential conflicts of interest.

REFERENCES

1 Benito AI, Diaz MA, Gonzalez-Vicent M et al. Hematopoietic stem cell transplantation using umbilical cord blood progenitors: Review of current clinical results. Bone Marrow Transplant 2004;33:675–690.

2 Devine SM, Lazarus HM, Emerson SG. Clinical application of hematopoietic progenitor cell expansion: Current status and future prospects. Bone Marrow Transplant 2003;31:241–252.

3 Heike T, Nakahata T. Ex vivo expansion of hematopoietic stem cells by cytokines. Biochim Biophys Acta 2002;1592:313–321.

4 Ueda T, Tsuji K, Yoshino H et al. Expansion of human NOD/SCID-repopulating cells by stem cell factor, Flk2/Flt3 ligand, thrombopoietin, IL-6, and soluble IL-6 receptor. J Clin Invest 2000;105:1013–1021.

5 Shpall EJ, Quinones R, Giller R et al. Transplantation of ex vivo expanded cord blood. Biol Blood Marrow Transplant 2002;8:368–376.

6 Jaroscak J, Goltry K, Smith A et al. Augmentation of umbilical cord blood (UCB) transplantation with ex vivo-expanded UCB cells: Results of a phase 1 trial using the AastromReplicell System. Blood 2003;101: 5061–5067.

7 Brandon C, Eisenberg LM, Eisenberg CA. WNT signaling modulates the diversification of hematopoietic cells. Blood 2000;96:4132–4141.

8 Murdoch B, Chadwick K, Martin M et al. Wnt-5A augments repopulating capacity and primitive hematopoietic development of human blood stem cells in vivo. Proc Natl Acad Sci U S A 2003;100:3422–3427.

9 Reya T, Duncan AW, Ailles L et al. A role for Wnt signalling in self-renewal of haematopoietic stem cells. Nature 2003;423:409–414.

10 Willert K, Brown JD, Danenberg E et al. Wnt proteins are lipid-modified and can act as stem cell growth factors. Nature 2003;423:448–452.

11 Bhatia M, Bonnet D, Wu D et al. Bone morphogenetic proteins regulate the developmental program of human hematopoietic stem cells. J Exp Med 1999;189:1139–1148.

12 Bhardwaj G, Murdoch B, Wu D. Sonic hedgehog induces the proliferation of primitive human hematopoietic cells via BMP regulation. Nat Immunol 2001;2:178–180.

13 Varnum-Finney B, Xu L, Brashem-Stein C et al. Pluripotent, cytokine-dependent, hematopoietic stem cells are immortalized by constitutive Notch1 signaling. Nat Med 2000;6:1278–1281.

14 Karanu FN, Murdoch B, Gallacher L et al. The notch ligand jagged-1 represents a novel growth factor of human hematopoietic stem cells. J Exp Med 2000;192:1365–1372.

15 Ohishi K, Varnum-Finney B, Bernstein ID. Delta-1 enhances marrow and thymus repopulating ability of human CD34(+)CD38(–) cord blood cells. J Clin Invest 2002;110:1165–1174.

16 Antonchuk J, Sauvageau G, Humphries RK. HOXB4-induced expansion of adult hematopoietic stem cells ex vivo. Cell 2002;109:39–45.

17 Lessard J, Sauvageau G. Bmi-1 determines the proliferative capacity of normal and leukaemic stem cells. Nature 2003;423:255–260.

18 Park IK, Qian D, Kiel M et al. Bmi-1 is required for maintenance of adult self-renewing haematopoietic stem cells. Nature 2003;423:302–305.

19 Amsellem S, Pflumio F, Bardinet D et al. Ex vivo expansion of human hematopoietic stem cells by direct delivery of the HOXB4 homeoprotein. Nat Med 2003;9:1423–1427.

20 Krosl J, Austin P, Beslu N et al. In vitro expansion of hematopoietic stem cells by recombinant TAT-HOXB4 protein. Nat Med 2003;9:1428–1432.

21 Buske C, Feuring-Buske M, Abramavich C et al. Deregulated expression of HOXB4 enhances the primitive growth activity of human hematopoietic cells. Blood 2002;100:862–868.

22 Brun AC, Fan X, Bjornsson JM et al. Enforced adenoviral vector-mediated expression of HOXB4 in human umbilical cord blood CD34+ cells promotes myeloid differentiation but not proliferation. Mol Ther 2003;8:618–628.

23 Magli MC, Largman C, Lawrence HJ. Effects of HOX homeobox genes in blood cell differentiation. J Cell Physiol 1997;173:168–177.

24 Buske C, Humphries RK. Homeobox genes in leukemogenesis. Int J Hematol 2000;71:301–308.

25 Lawrence HJ, Helgason CD, Sauvageau G et al. Mice bearing a targeted interruption of the homeobox gene HOXA9 have defects in myeloid, erythroid, and lymphoid hematopoiesis. Blood 1997;89: 1922–1930.

26 Dorsam ST, Ferrell CM, Dorsam GP et al. The transcriptome of the leukemogenic homeoprotein HOXA9 in human hematopoietic cells. Blood 2004;103:1676–1684.

27 Crooks GM, Fuller J, Petersen D et al. Constitutive HOXA5 expression inhibits erythropoiesis and increases myelopoiesis from human hematopoietic progenitors. Blood 1999;94:519–528.

28 Bromleigh VC, Freedman LP. p21 is a transcriptional target of HOXA10 in differentiating myelomonocytic cells. Genes-Dev 2000; 14:2581–2586.

29 Bjornsson JM, Andersson E, Lundstrom P et al. Proliferation of primitive myeloid progenitors can be reversibly induced by HOXA10. Blood 2001;98:3301–3308.

30 Zimmermann F, Rich IN. Mammalian homeobox B6 expression can be correlated with erythropoietin production sites and erythropoiesis during development, but not with hematopoietic or nonhematopoietic stem cell populations. Blood 1997;89:2723–2735.

31 Mann RS, Affolter M. Hox proteins meet more partners. Curr Opin Genet Dev 1998;8:423–429.

32 Pineault N, Helgason CD, Lawrence HJ et al. Differential expression of Hox, Meis1, and Pbx1 genes in primitive cells throughout murine hematopoietic ontogeny. Exp Hematol 2002;30:49–57.

33 Di Rocco G, Mavilio F, Zappavigna V. Functional dissection of a transcriptionally active, target-specific Hox-Pbx complex. EMBO J 1997;16:3644–3654.

Hematopoietic stem cell–engrafted NOD/SCID/IL2Rγ^{null} mice develop human lymphoid systems and induce long-lasting HIV-1 infection with specific humoral immune responses

Satoru Watanabe,[1] Kazuo Terashima,[2] Shinrai Ohta,[3] Shigeo Horibata,[3] Misako Yajima,[4] Yoko Shiozawa,[1] M. Zahidunnabi Dewan,[2,3] Zhong Yu,[2] Mamoru Ito,[5] Tomohiro Morio,[6] Norio Shimizu,[1] Mitsuo Honda,[3] and Naoki Yamamoto[2,3]

[1]Department of Virology, Division of Medical Science, Medical Research Institute, Tokyo Medical and Dental University, Japan; [2]Department of Molecular Virology, Graduate School of Medicine, Tokyo Medical and Dental University, Japan; [3]AIDS Research Center, National Institute of Infectious Diseases, Tokyo, Japan; [4]Department of Infectious Diseases, National Research Institute for Child Health and Development, Tokyo, Japan; [5]Central Institute for Experimental Animals, Kanagawa, Japan; and [6]Department of Pediatrics and Developmental Biology, Graduate School of Medicine, Tokyo Medical and Dental University, Japan

Critical to the development of an effective HIV/AIDS model is the production of an animal model that reproduces long-lasting active replication of HIV-1 followed by elicitation of virus-specific immune responses. In this study, we constructed humanized nonobese diabetic/severe combined immunodeficiency (NOD/SCID)/interleukin-2 receptor γ-chain knockout (IL2Rγ^{null}) (hNOG) mice by transplanting human cord blood–derived hematopoietic stem cells that eventually developed into human B cells, T cells, and other monocytes/macrophages and dendritic cells associated with the generation of lymphoid follicle–like structures in lymphoid tissues. Expressions of CXCR4 and CCR5 antigens were recognized on CD4$^+$ cells in peripheral blood, the spleen, and bone marrow, while CCR5 was not detected on thymic CD4$^+$ T cells. The hNOG mice showed marked, long-lasting viremia after infection with both CCR5- and CXCR4-tropic HIV-1 isolates for more than the 40 days examined, with R5 virus–infected animals showing high levels of HIV-DNA copies in the spleen and bone marrow, and X4 virus–infected animals showing high levels of HIV-DNA copies in the thymus and spleen. Furthermore, we detected both anti–HIV-1 Env gp120– and Gag p24–specific antibodies in animals showing a high rate of viral infection. Thus, the hNOG mice mirror human systemic HIV infection by developing specific antibodies, suggesting that they may have potential as an HIV/AIDS animal model for the study of HIV pathogenesis and immune responses. (Blood. 2007; 109:212-218)

Introduction

Current animal models for either human immunodeficiency virus type 1 (HIV-1) or simian immunodeficiency virus (SIV) suffer from the lack of a system precisely mirroring human HIV infection and the progression to disease state.[1] In current animal models with HIV infection, such as chimpanzees, animals do not develop AIDS.[1] Past animal models for HIV infection have relied on humanized severe combined immunodeficiency (hSCID) mice models to study prospective anti-HIV drugs and vaccines. SCID-hu (Thy/Liv) mice, engrafted with human fetal thymus and liver tissue in the renal subcapsular region, were first reported as the small-animal model.[2] Because human T cells are generated within the engrafted thymus, this model has been used for the study of thymopoiesis[3-6] and hematopoiesis[7,8] under the burden of HIV-1 infection. However, this model allows for a limited systemic HIV-1 infection, which is restricted mainly to the engrafted thymus. Another HIV mouse model, hu-PBL–SCID mice engrafted with human peripheral blood mononuclear cells (PBMCs),[9] has been actively used as a tool in developing antiretroviral therapy.[9-11] However, the infection persists for only a short time in association with rapid loss of CD4$^+$ T cells because there is no active hematopoiesis or thymopoiesis.[9,12,13] Furthermore, these mouse models fail to mirror certain key aspects of the human immune response, lacking normal lymphoid tissue and functional human antigen-presenting cells such as dendritic cells (DCs).[14] Thus, although these mouse models are valuable as animal models for HIV infection, the development of a mouse model more analogous to human HIV infection is needed if we are to better understand HIV pathogenesis and develop successful anti-HIV therapies and preventive vaccines.

To solve the difficult issue about the development of an ideal HIV mouse model, we initially selected a humanized nonobese diabetic (NOD)/SCID interleukin-2 receptor (IL-2R) γ-chain knockout (NOG) mouse[15] as a model animal because it has been suggested that multilineage cells, including human T, B, and natural killer (NK) cells, differentiate in these mice when given transplants of human CD34$^+$ hematopoietic stem cells.[16-18] In the current study, we further reveal the kinetics of differentiation of human B and T cells, monocytes/macrophages, and DCs in the mice that received transplants, and we characterize the animals by infection with both CCR5 (R5)– and CXCR4 (X4)-tropic HIV strains. Since our hNOG mice show stable and systemic infection of both R5- and X4-tropic HIV for more than

Submitted April 20, 2006; accepted August 12, 2006. Prepublished online as *Blood* First Edition Paper, September 5, 2006; DOI 10.1182/blood-2006-04-017681.

The publication costs of this article were defrayed in part by page charge payment. Therefore, and solely to indicate this fact, this article is hereby marked "advertisement" in accordance with 18 USC section 1734.

34 Asahara H, Dutta S, Kao HY et al. Pbx-Hox heterodimers recruit coactivator-corepressor complexes in an isoform-specific manner. Mol Cell Biol 1999;19:8219–8225.

35 Saleh M, Rambaldi I, Yang XJ et al. Cell signaling switches HOX-PBX complexes from repressors to activators of transcription mediated by histone deacetylases and histone acetyltransferases. Mol Cell Biol 2000; 20:8623–8633.

36 Lu Y, Goldenberg I, Bei L et al. HoxA10 represses gene transcription in undifferentiated myeloid cells by interaction with histone deacetylase 2. J Biol Chem 2003;278:47792–47802.

37 Phelan ML, Rambaldi I, Featherstone MS. Cooperative interactions between HOX and PBX proteins mediated by a conserved peptide motif. Mol Cell Biol 1995;15:3989–3997.

38 Piper DE, Batchelor AH, Chang CP et al. Structure of a HoxB1-Pbx1 heterodimer bound to DNA: Role of the hexapeptide and a fourth homeodomain helix in complex formation. Cell 1999;96:587–597.

39 Shanmugam K, Featherstone MS, Saragovi HU. Residues flanking the HOX YPWM motif contribute to cooperative interactions with PBX. J Biol Chem 1997;272(30):19081–19087.

40 Sprules T, Green N, Featherstone M et al. Conformational changes in the PBX homeodomain and C-terminal extension upon binding DNA and HOX-derived YPWM peptides. Biochemistry 2000;39:9943–9950.

41 LaRonde-LeBlanc NA, Wolberger C. Structure of HoxA9 and Pbx1 bound to DNA: Hox hexapeptide and DNA recognition anterior to posterior. Genes Dev 2003;17:2060–2072.

42 Krosl J, Beslu N, Mayotte N et al. The competitive nature of HOXB4-transduced HSC is limited by PBX1: the generation of ultra-competitive stem cells retaining full differentiation potential. Immunity 2003;18:561–571.

43 Beslu N, Krosl J, Laurin M et al. Molecular interactions involved in HOXB4-induced activation of HSC self-renewal. Blood 2004;104: 2307–2314.

44 Tanaka H, Matsumura I, Ezoe S et al. E2F1 and c-Myc potentiate apoptosis through inhibition of NF-kappaB activity that facilitates Mn-SOD-mediated ROS elimination Mol Cell 2002;9:1017–1029.

45 Cannon MJ, Papalia GA, Navratilova I et al. Comparative analyses of a small molecule/enzyme interaction by multiple users of Biacore technology. Anal Biochem 2004;330:98–113.

46 Tajima S, Tsuji K, Ebihara Y et al. Analysis of interleukin 6 receptor and gp130 expressions and proliferative capability of human CD34+ cells. J Exp Med 1996;184:1357–1364.

47 Bhatia M, Bonnet D, Kapp U et al. Quantitative analysis reveals expansion of human hematopoietic repopulating cells after short-term ex vivo culture. J Ex Med 1997;186:619–624.

48 Wang JC, Doedens M, Dick JE. Primitive human hematopoietic cells are enriched in cord blood compared with adult bone marrow or mobilized peripheral blood as measured by the quantitative in vivo SCID-repopulating cell assay. Blood 1997;89:3919–3924.

49 Satoh Y, Matsumura I, Tanaka H et al. Roles for c-Myc in self-renewal of hematopoietic stem cells. J Biol Chem 2004;279:24986–24993.

50 Matsumura I, Kitamura T, Wakao H et al. Transcriptional regulation of the cyclin D1 promoter by STAT5: its involvement in cytokine-dependent growth of hematopoietic cells. EMBO J 1999;18:1367–1377.

51 Matsumura I, Ishikawa J, Nakajima K et al. Thrombopoietin-induced differentiation of a human megakaryoblastic leukemia cell line, CMK, involves transcriptional activation of p21(WAF1/Cip1) by STAT5. Mol Cell Biol 1997;17:2933–2943.

52 Hodel MR, Corbett AH, Hodel AE. Dissection of a nuclear localization signal. J Biol Chem 2001;276:1317–1325.

53 Gao J, Mazella J, Tseng L. Hox proteins activate the IGFBP-1 promoter and suppress the function of hPR in human endometrial cells. DNA Cell Biol 2002;21:819–825.

54 Dorrell C, Gan OI, Pereira DS et al. Expansion of human cord blood CD34(+)CD38(–) cells in ex vivo culture during retroviral transduction without a corresponding increase in SCID repopulating cell (SRC) frequency: Dissociation of SRC phenotype and function. Blood 2000;95: 102–110.

55 Brun AC, Bjornsson JM, Magnusson M et al. Hoxb4-deficient mice undergo normal hematopoietic development but exhibit a mild proliferation defect in hematopoietic stem cells. Blood 2004;103:4126–4133.

56 Björnsson JM, Larsson N, Brun AC et al. Reduced proliferative capacity of hematopoietic stem cells deficient in Hoxb3 and Hoxb4. Mol Cell Biol 2003;23:3872–3883.

57 Knoepfler PS, Sykes DB, Pasillas M et al. HoxB8 requires its Pbx-interaction motif to bl7ck differentiation of primary myeloid progenitors and of most cell line models of myeloid differentiation. Oncogene 2001;20:5440–5448.

58 Kroon E, Thorsteinsdottir U, Mayotte N et al. NUP98-HOXA9 expression in hemopoietic stem cells induces chronic and acute myeloid leukemias in mice. EMBO J 2001;20:350–361.

59 Noguchi H, Matsushita M, Okitsu et al. A new cell-permeable peptide allows successful allogeneic islet transplantation in mice. Nat Med 2004;10:305–309.

60 Kaneto H, Nakatani Y, Miyatsuka T et al. Possible novel therapy for diabetes with cell-permeable JNK-inhibitory peptide. Nat Med 2004;10: 1128–1132.

61 DiMartino JF, Selleri L, Traver D et al. The Hox cofactor and proto-oncogene Pbx1 is required for maintenance of definitive hematopoiesis in the fetal liver. Blood 2001;98:618–626.

62 Furukawa U, Kikuchi J, Nakamura M et al. Lineage-specific regulation of cell cycle control gene expression during haematopoietic cell differentiation. Br J Haematol 2000;110:663–673.

63 Cheng T, Rodrigues N, Shen H et al. Hematopoietic stem cell quiescence maintained by p21cip1/waf1. Science 2000;287:1804–1808.

64 Yuan Y, Shen H, Franklin DS et al. In vivo self-renewing divisions of haematopoietic stem cells are increased in the absence of the early G1-phase inhibitor, p18INK4C. Nat Cell Biol 2004;6:436–442.

65 Ito K, Hirao A, Arai F et al. Regulation of oxidative stress by ATM is required for self-renewal of haematopoietic stem cells. Nature 2004;431: 997–1002.

66 Cheng T, Rodrigues N, Dombkowski D et al. Stem cell repopulation efficiency but not pool size is governed by p27(kip1). Nat Med 2000;6: 1235–1240.

the 40 days studied, and HIV-specific antibodies are detectable in the animals with high plasma viral loads and HIV-DNA copy numbers, we also discuss the suitability of HIV-hNOG mice as an animal model for HIV-1 infection.

Materials and methods

Transplantation of human CB-derived hematopoietic stem cells in NOG mice

Human cord blood (CB) was obtained from Saiseikai Central hospital (Minato-ku, Tokyo, Japan) and Tokyo Cord Blood Bank (Katsushika-ku, Tokyo, Japan) after obtaining informed consent. All research on human subjects was approved by the Institutional Review Board of each institution participating in the project. CB mononuclear cells were separated by Ficoll-Hypaque density gradient. $CD34^+$ hematopoietic stem cells were isolated using a magnetic-activated cell sorting (MACS) Direct CD34 Progenitor Cell Isolation Kit (Miltenyi Biotec, Bergisch Gladbach, Germany) according to the manufacturer's instructions. More than 95% of $CD34^+$ cells were positively selected after 2 time-enrichment manipulations. Cells were either immediately used for the transplantation or frozen until use. NOG mice were obtained from the Central Institute for Experimental Animals (Kawasaki, Japan) and maintained under specific pathogen–free (SPF) conditions in the animal facility of the National Institute of Infectious Diseases (NIID; Tokyo, Japan). Mice used in these studies were free of known pathogenic viruses, herpes viruses, bacteria, and parasites. They were housed in accordance with the Guidelines for Animal Experimentation of the Japanese Association for Laboratory Animal Science (1987) under the Japanese Law Concerning the Protection and Management of Animals, and were maintained in accordance with the guidelines set forth by the Institutional Animal Care and Use Committee of NIID, Japan. Once approved by the Institutional Committee for Biosafety Level 3 experiments, these studies were conducted at the Animal Center, NIID, Japan, in accordance with the requirements specifically stated in the laboratory biosafety manual of the World Health Organization. Female mice (6 to 10 weeks old) were irradiated (300 cGy) and 1×10^4 to 1.2×10^5 $CD34^+$ cells were intravenously injected within 12 hours.

Flow cytometry

The purity of CB-derived $CD34^+$ cells after separation was evaluated by double staining with FITC-conjugated anti–human CD45 (J.33) and PE-conjugated anti–human CD34 (Class III 581) (all from Beckman Coulter, Fullerton, CA). After transplantation (1-7 months), peripheral blood, spleens, bone marrow (BM), and thymi were collected for flow cytometric analysis following staining with the following monoclonal antibodies (mAbs): FITC-conjugated anti–human CD45 (J.33), CD3 (UCHT1), CD4 (13B8.2), CD19 (J4.119), CD45RO (UCHL1) (all from Beckman Coulter), and CCR5 (2D7; BD Pharmingen, San Diego, CA); PE-conjugated anti–human CD4 (13B8.2), CD8 (B9.11), CD19 (J4.119), CD45RA (ALB11) (all from Beckman Coulter), and CXCR4 (44717; R&D Systems, Minneapolis, MN); anti–mouse CD45 (YW62.3; Beckman Coulter); ECD-conjugated anti–human CD45 (J.33; Beckman Coulter); and PC5-conjugated anti–human CD8 (T8) and CD14 (Rm052) (all from Beckman Coulter). Flow cytometric analysis was conducted by 2- or 4-color staining using an EpicsXL (Beckman Coulter).

Immunohistochemistry

Organs were snap-frozen following embedding in OCT compound (Sakura Finetechnical, Tokyo, Japan). Frozen sections were air-dried and fixed in acetone. HIV-1–infected organs were fixed in 4% paraformaldehyde and embedded in OCT compound following immersion in gradient sucrose (5%-30%). Fixed samples were stained with the following mAbs: anti–human CD45 (1.22/4014; Nichirei, Tokyo, Japan), CD3 (UCHT1; DAKO, Glostrup, Denmark), CD20 (L26; DAKO), CD68 (KP1; DAKO), CD205 (MG38; eBioscience, San Diego, CA), and DRC-1 (R4/23; DAKO) for follicular dendritic cells (FDCs); anti–mouse FDC-M1 (BD Pharmingen) for murine FDCs; and HIV-1 Gag p24 (DAKO) for detection of infected cells. Biotin-labeled goat $F(ab')_2$ anti–mouse immunoglobulin (Ig; ICN Biomedicals, Aurora, OH)– or biotin-labeled mouse $F(ab')_2$ anti–rat IgG (Jackson ImmunoResearch Laboratories, West Grove, PA) was used as the secondary antibody. Samples were treated with alkaline phosphatase (AP) or horseradish peroxidase (HRP)–streptavidin conjugate (ZYMED Laboratories Inc, San Francisco, CA). BCIP/NBT, DAB, or AEC (all from DAKO) was used for the visualization. Photographs were taken by light microscopy (Leica DMRA; Leica Microsystems Wetzlar, Wetzlar, Germany) using Leica HC PLAN APO lenses (10×/0.40 NA PH1). Leica Q550 was used for image processing.

Measurement of human Igs in mice plasma

Plasma concentrations of human IgM, IgG, and IgA in NOG mice that received transplants of human stem cells were determined by conventional human Ig quantitation assay at BML Inc (Tokyo, Japan).

Cells and viruses

Human embryonic kidney 293T cells and monkey kidney COS7 cells were cultured in RPMI 1640 supplemented with 10% fetal bovine serum (FBS) and antibiotics. The 293T cells and COS7 cells were used for transfection of DNA plasmids containing HIV-1_{JRCSF} and simian/human immunodeficiency virus (SHIV)–C2/1, respectively. The SHIV-C2/1 strain contains the *env* gene of pathogenic HIV-1 strain 89.6.[19] Cell-free supernatant was collected and stored at −80°C before use. A primary clinical isolate, HIV-1_{MNp}, was kindly provided by Dr J. Sullivan of the University of Massachusetts Medical School (Worcester, MA). PBMCs isolated from HIV-1–seronegative individuals were cultured in RPMI 1640 supplemented with 10% FBS and antibiotics with 5 μg of phytohemagglutinin (PHA)/mL for 3 or 7 days (PHA-PBMCs). HIV-1_{MNp} was propagated in PHA-PBMCs, and cell-free virus stocks were stored at −80°C.

The 50% tissue-culture infectious dose ($TCID_{50}$) was determined using PHA-PBMCs and the endpoint dilution method. A 4-fold series of dilution was prepared from the virus stock, and then cells were mixed and cultured for 7 days for X4–HIV-1 and 14 days for R5–HIV-1 in RPMI 1640 supplemented with 20% FBS and antibiotics. The endpoints were determined by screening for the p24 antigen using Lumipulse (Fujirevio, Tokyo, Japan).

HIV-1 infection

All procedures for the infection and maintenance of NOG mice were performed in Biosafety Level 3 facilities at NIID under standard caging conditions. On days 102 to 132 after stem cell transplantation, 16 mice were inoculated intravenously with R5-tropic HIV-1_{JRCSF} (65 000 $TCID_{50}$) or X4-tropic SHIV-C2/1 (50 000 $TCID_{50}$). On days 18 to 43 after inoculation, plasma was collected to determine HIV-RNA copy numbers, and spleen cells were prepared as single-cell suspensions to analyze the CD4/CD8 ratio using flow cytometry. A number (14) of other mice were inoculated intravenously with R5-tropic HIV-1_{JRCSF} (200 or 65 000 $TCID_{50}$) or X4-tropic HIV-1_{MNp} (180 or 20 000 $TCID_{50}$) on days 126 to 146 after transplantation. On days 18 to 40 after inoculation, plasma was collected for the determination of HIV-RNA copy numbers, and single-cell suspensions of the spleen, BM, and thymus were prepared for HIV-DNA measurement. The CD4/CD8 ratio in the spleen and percentages of human $CD45^+$ cells in organs were analyzed using flow cytometry.

Virologic analysis

Plasma viral RNA copy numbers were measured using a real-time quantification assay based on the TaqMan system (Applied Biosystems, Foster City, CA). Plasma viral RNA was extracted and purified using a QIAamp Viral RNA Mini Kit (Qiagen, Valencia, CA). The RNA was subjected to reverse transcription (RT) and amplification using a TaqMan One-Step RT–polymerase chain reaction (PCR) Master Mix Reagents Kit (PE Biosystems, Foster City, CA) with HIV-1 gag consensus primers

(forward, 5′-GGACATCAAGCAGCCATGCAA-3′; and reverse, 5′-TGCTATGTCACTTCCCCTTGG-3′) and an HIV-1 gag consensus TaqMan probe (FAM-5′-ACCATCAATGAGGAAGCTGCAGAA-3′-TAMRA). For SHIV-C2/1 analysis, primers (forward, 5′-AATGCAGAGCCCCAAGAAGAC-3′; and reverse, 5′-GGACCAAGGCCTAAAAAACCC-3′) and a TaqMan probe (FAM-5′-ACCATGTTATGGCCAAATGCCCAGAC-3′-TAMRA) were designed for targeting the SIVmac239 gag region.[20] Probed products were quantitatively monitored by their fluorescence intensity with the ABI7300 Real-Time PCR system (PE Biosystems). To obtain control RNA for quantification, HIV-1 gag RNA and SIVmac239 gag RNA were synthesized using T7 RNA polymerase and pKS460. Viral DNA was extracted and purified using a QIAamp DNA Mini Kit (Qiagen). Determination of HIV-1 DNA copy numbers was performed by real-time PCR assay with TaqMan Master mixture (PE Biosystems). Primers (forward, 5′-GGCTAACTAGGGAACCCACTG-3′; and reverse, 5′-CTGCTAGAGATTTTCCACACT-3′) and probes (FAM-5′-TAGTGTGTGCCCGTCTGTTGTGTGAC-3′-TAMRA) were designed for targeting the HIV-1 long terminal repeat region, R/U5. The viral DNA was quantified using LightCycler (Roche Diagnostics, Almere, The Netherlands). Viral RNA and DNA were calculated based on the standard curve of control RNA and DNA. All assays were carried out in duplicate.

HIV-antigen ELISA

Levels of anti–HIV-1 Igs against recombinant HIV-1_{IIIB} Env gp120, recombinant HIV-1_{MN} Env gp120, and recombinant HIV-1_{IIIB} Gag p24 (all from ImmunoDiagnostics Inc, Woburn, MA) in plasma from HIV-1–infected and –uninfected control mice were determined using a standard enzyme-linked immunosorbent assay (ELISA). Microplates (96-well) were coated overnight with 200 ng/well antigens, and plasma diluted 1:20, 1:60, and 1:180 with PBS were incubated for 1 hour. AP-labeled anti–human Igs (γ, α, and μ; Sigma-Aldrich, St Louis, MO) were used as secondary antibodies. P-nitrophenylphosphate (pNPP) Solution (WAKO Chemical USA, Richmond, VA) was used for the visualization. The enzyme reaction was stopped by addition of 0.1 M NaOH and read at 405 nm. All assays were carried out in triplicate.

Statistical analysis

Data were expressed as the mean value ± standard deviation (SD). Significant differences between data groups were determined by 2-sample Student *t* test analysis. A *P* value less than .05 was considered significant.

Results

Reconstitution of human lymphoid systems in hNOG mice

The initial studies describing the construction of humanized SCID mice used the human PBMC for infection of immunodeficiency viruses.[9,12,21] However, these hu-PBL-SCID mice showed a partial infection to the R5 virus and a relatively limited period of viral replication. To construct a more suitable mouse model mimicking HIV-1 infection in humans, we selected human CB stem cells as a transplant for NOG mice. NOG mice were inoculated intravenously with human $CD34^+$ hematopoietic stem cells, and their development of human lymphoid systems were then monitored. After transplantation (2 months), human $CD45^+$ leukocytes were recognized in both PB and the spleen, but most of the cells were human B cells (Figure 1A). Human T cells began to be recognized clearly in PB and the spleen 4 months after transplantation (Figure 1B) and gradually increased in level, as did human B cells (Figure 1C).

In Figure 1D, we summarized percentages of human $CD3^+$ T cells in human $CD45^+$ cells from 38 mice from 39 to 213 days after transplantation. Human $CD3^+$ T cells clearly increased 100 days after transplantation in both PB and the spleen. After transplantation (4 months), human $CD3^+$ T cells in the spleen preferably expressed CD45RA rather than CD45RO (70.8% ± 13.4% and 27.3% ± 38.8% in $CD3^+$ T cells, respectively; n = 5; Figure 1E), demonstrating that most of the T cells were in a naive state. In addition, plasma taken from 5 mice 113 to 143 days after transplantation showed that all mice produced human IgM, with concentrations ranging from 0.025 to 0.5 g/L, and that human IgG and IgA was also detected in some of the mice (ranges, 0.015-0.18 g/L and 0.003-0.012 g/L, respectively) (data not shown).

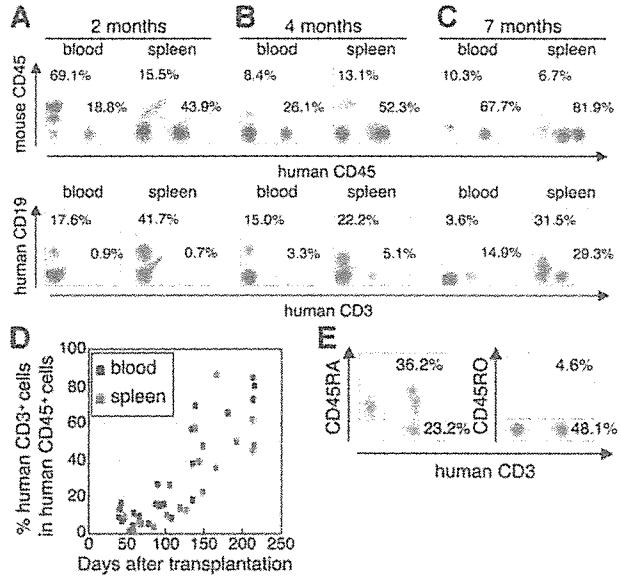

Figure 1. Flow cytometric analysis of human T cells in the peripheral blood and spleen in NOG mice given intravenous transplants of human CB-derived $CD34^+$ cells. (A-C) Representative profiles of the mice 2 months (A), 4 months (B), and 7 months (C) after transplantation. The ratio of human to murine $CD45^+$ cells and that of human $CD3^+$ to $CD19^+$ cells show an incremental increase in human $CD45^+$ cells and human $CD3^+$ cells from 2 to 7 months. (D) Change of net percentages of human $CD3^+$ T cells among human $CD45^+$ cells in peripheral blood and the spleen from 38 mice 39 to 213 days after transplantation. (E) CD45RA is more efficiently expressed than CD45RO on human $CD3^+$ T cells in spleen. A gate was set on the human $CD45^+$ population. The fluorescence-activated cell sorting (FACS) profile is representative of 1 in a group of 5 mice.

By 7 months after transplantation, human $CD45^+$ leukocytes comprised more than 80% to 90% of mononuclear cells in the spleen (Figure 1C), and most of the mice showed symptoms of a wasting condition and a hunched back. Based upon these results, we determined that the suitable period for HIV inoculation would be 4 to 5 months after transplantation.

Formation of lymphoid structures, including monocytes/macrophages, DCs, and FDCs

Next, using the hNOG mice at 4 months after transplantation, we investigated lymphoid structure formation and the development of human monocytes, macrophages, DCs, and FDCs, which are very important factors not only for elicitation of immune responses against foreign antigens, but also for the spread of HIV-1 infection in a body.[22-24] Human $CD14^+$ monocytes were detected in PB, the spleen, and BM using flow cytometry (Figure 2A). During immunohistochemical analysis, human $CD45^+$ leukocytes gathered in a form of follicle-like structures (FLSs) at the end of the central artery in the spleen (Figure 2B). From a serial section of the same region (Figure 2B-G), these structures consisted mainly of human $CD20^+$ B cells (Figure 2C) admixed with a small number of human $CD3^+$ T cells (Figure 2D). Hardly any human FDCs positive for DRC-1 were detected (data not shown), whereas a

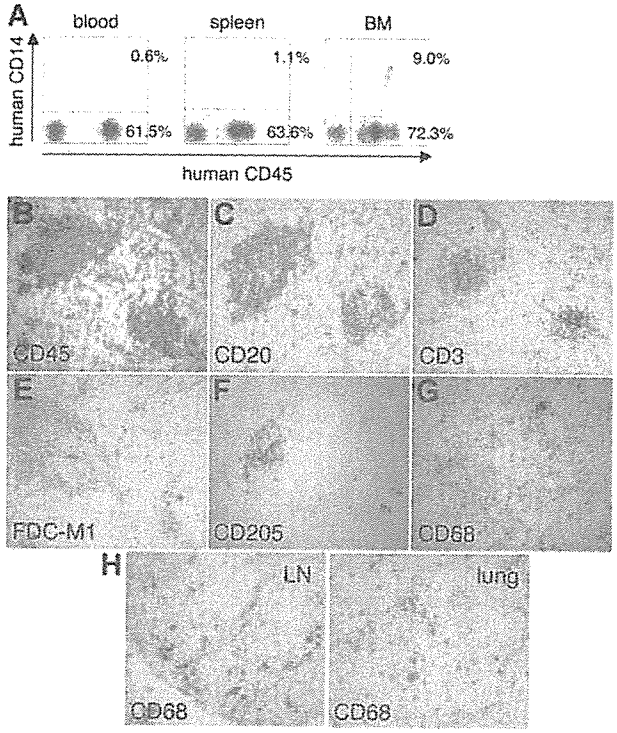

Figure 2. Flow cytometric analysis and immunohistochemical analysis of the expression of myelomonocytic markers in hNOG mice 4 months after transplantation. (A) Human CD14$^+$ monocytes/macrophages are recognized in peripheral blood, the spleen, and BM. (B-G) Immunohistochemical findings from serially sectioned spleen for the expressions of human CD45 (B), human CD20 (C), human CD3 (D), murine FDC (E), human CD205 (F), and human CD68 (G). (H) Human CD68$^+$ macrophages are also detected in the medulla of the LN and lung. Visualization was performed with BCIP (B-D, F-G), DAB (E), and AEC (H). Original magnification, ×100.

loose network of murine FDCs positive for FDC-M1 was recognized in the distal portion of the FLSs (Figure 2E). Human CD205$^+$ DCs were predominantly detected in a cluster form within the FLSs (Figure 2F), while human CD68$^+$ macrophages were scattered throughout the spleen (Figure 2G). Many human CD68$^+$ macrophages were also observed in various other organs, including the lymph nodes (LNs) and the lungs (Figure 2H).

Expression of HIV-1 coreceptors on CD4$^+$ cells in various tissues

Since the development of lymphoid tissues was recognized in hNOG mice, we focused on the expressions of HIV-1 coreceptors CXCR4 and CCR5 on human CD4$^+$ cells in these tissues. CXCR4 antigen was expressed in 36.5% ± 4.2% (n = 4) of the CD4$^+$ cells in PB (Figure 3A) and 78.1% ± 17.1% (n = 5) in the spleen (Figure 3B). CCR5$^+$ cells were detected in 15.5% ± 1.8% (n = 4) of CD4$^+$ cells in PB and 28.6% ± 12.6% (n = 5) in the spleen (Figure 3A-B). In the thymus, CD4$^+$CD8$^+$ thymocytes existed in 82.9% ± 4.4% (n = 5) as well as small numbers of CD4$^+$CD8$^-$ cells (6.4% ± 2.4%; n = 5) and CD4$^-$CD8$^+$ cells (7.7% ± 3.0%; n = 5), with the CXCR4 antigen expressed in 50.1% ± 4.5% (n = 5) of CD4$^+$ cells, while, as with normal human thymocytes,[25] CCR5$^+$ cells were almost undetectable, with less than 1% (0.6% ± 0.1%; n = 5) (Figure 3C). Human CD3$^+$ T cells and CD14$^+$ monocytes in BM were detected only in 3.2% ± 2.1% and 5.8% ± 3.8%, respectively, while CD4$^+$ cells were recognized in 18.1% ± 6.5%, with many expressing both CXCR4 (75.0% ± 23.1%) and CCR5 (81.3% ± 6.6%; n = 5; Figure 3D). Thus, distributions of HIV-1 coreceptor–positive cells in these lymphoid tissues suggest that the hNOG mice allow for sufficient development of human cells to make the study of HIV-1 pathogenesis possible.

Both R5- and X4-tropic HIVs efficiently infect and replicate in hNOG mice

In our preliminary study, using low and high doses of challenge virus, no viral infection was detected in any of the virus-inoculated hNOG mice at 7 days after infection, while some showed detectable plasma viral loads at 14 days (data not shown). Then, we prepared 16 hNOG mice that received transplants of stem cells and inoculated them with a high dose of R5-tropic HIV-1_{JRCSF} (65 000 $TCID_{50}$) and X4-tropic SHIV-C2/1 (50 000 $TCID_{50}$) intravenously through the tail vein at 102 to 132 days after transplantation. Upon HIV-1_{JRCSF} infection, viral copy numbers in plasma rose to a level of 1.6×10^5 to 5.8×10^5 copies/mL (n = 4) on day 33 and 2.0×10^5 to 4.7×10^5 copies/mL on day 43 (n = 4) (Figure 4A). Moreover, for SHIV-C2/1 infection, viral copy numbers in plasma were 1.6×10^3 to 3.2×10^5 copies/mL on day 18 (n = 4) and reached 5.4×10^4 to 1.1×10^5 copies/mL on day 42 (n = 4; Figure 4B). In these mice, no significant decline in the CD4/CD8 ratio was observed throughout entire period of follow-up for the R5-tropic virus infection, while CD4$^+$ cell decline was detected for the X4-tropic virus infection on day 42 after infection ($P = .044$) but not on day 18 after infection (Figure 4C). Four mice that did not receive transplants of human stem cells showed no detectable levels of plasma viral load (less than 500 copies/mL) following HIV/SHIV inoculation (data not shown).

To confirm HIV infection, we used immunohistochemistry to detect the presence of the p24 antigen of the HIV-1 Gag protein in various tissues of mice showing viremia. p24$^+$ cells were clearly identified in the spleen, LN, and lungs (Figure 4D), which include macrophage-like cells.

Different distributions of R5- and X4-tropic viruses in lymphoid tissues

A number of mice (14) were further analyzed for HIV-1 infection on days 126 to 146 after transplantation with a low dose (200 $TCID_{50}$) or a high dose (65 000 $TCID_{50}$) of R5-tropic HIV-1_{JRCSF} and a low dose (180 $TCID_{50}$) or a high dose (20 000 $TCID_{50}$) of X4-tropic HIV-1_{MNp}. Consequently, 2 of the 4 mice given a low

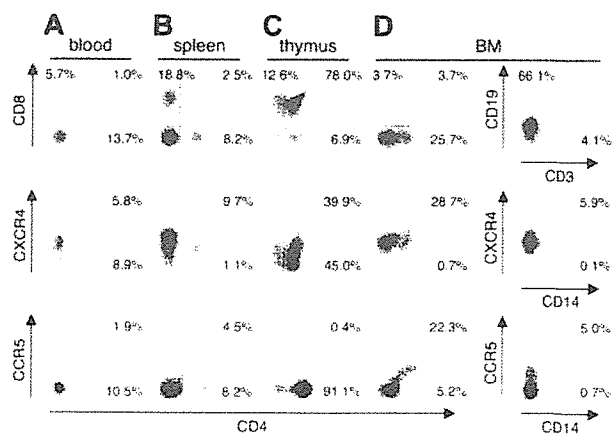

Figure 3. Surface expression of HIV-1 coreceptors on CD4$^+$ cells in various organs of mice 4 months after transplantation. A representative FACS profile of human CXCR4 and CCR5 on CD4$^+$ cells shows the existence of CXCR4$^+$CD4$^+$ and CCR5$^+$CD4$^+$ cells in blood (A), spleen (B), and BM (D), but no CCR5$^+$CD4$^+$ cells in the thymus (C). BM results show that many CD4$^+$ cells are neither CD3$^+$ T cells nor CD14$^+$ monocytes. A gate was set on the human CD45$^+$ population.

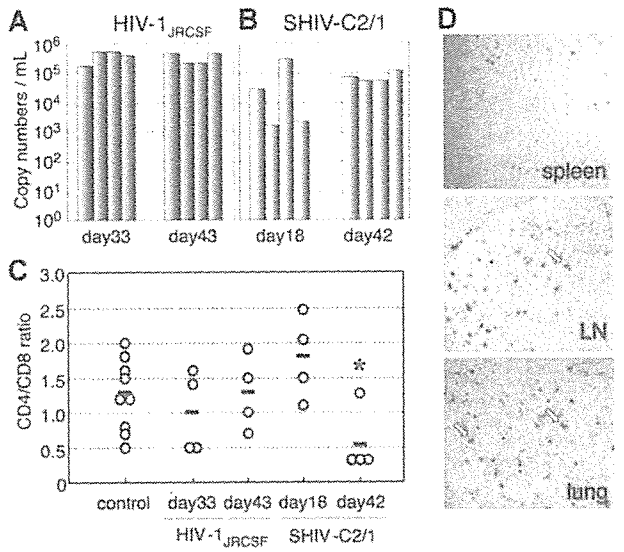

Figure 4. The numbers of RNA viral copies in plasma, CD4+/CD8+ T-cell ratios in the spleen, and p24 detection in the immunohistochemistry of HIV/SHIV-infected mice. (A) Viral copy numbers of 8 mice inoculated with a high infectious dose of HIV-1_{JRCSF} (65 000 $TCID_{50}$) and killed on days 33 and 43 after inoculation. (B) Viral copy numbers of 8 mice inoculated with a high infectious dose of SHIV-C2/1 (50 000 $TCID_{50}$) and killed on days 18 and 42 after inoculation. Note that all the mice showed high levels of viremia that lasted more than 40 days after inoculation. (C) CD4/CD8 cell ratios in the spleens of 16 infected mice and 9 uninfected control mice. Control mice were not inoculated with HIV/SHIV and were killed on days 105 to 166 after stem cell transplantation. There was no significant rapid loss of $CD4^+$ cells in HIV-1_{JRCSF}–infected mice, while a decline of the CD4/CD8 ratio was detected in SHIV-C2/1–infected mice on day 42 after infection compared with uninfected control mice (*$P < .05$). The short bars indicate the means of each group. (D) $P24^+$ cells are clearly observed in the spleen, LNs, and lungs. Arrow indicates p24 positive for macrophage-like cells. Original magnification, ×100.

dose of HIV-1_{JRCSF} and 2 of the 3 mice given a low dose of HIV-1_{MNp} were successfully infected (Table 1), suggesting that each dose represents an approximately 50% infectious dose of HIV for hNOG mice. High HIV-DNA copy numbers were mainly detected in the spleen and BM of the HIV-1_{JRCSF} –infected mice, and in the thymus and spleen of the HIV-1_{MNp}–infected mice, while their BM showed lower copy numbers (Table 1).

Generation of HIV-specific antibodies in hNOG mice at a high multiplicity of infection

We then tested for generation of human antibodies against HIV-1 from these 14 mice by HIV antigen-specific ELISA. The sera of mice no. 136-3 and no. 157-3 infected with HIV-1_{JRCSF} and HIV-1_{MNp}, respectively, showed significant levels of human antibodies specific for HIV-1_{IIIB}-Env gp120 (Figure 5A), HIV-1_{MN}-Env gp120 (Figure 5B), and HIV-1_{IIIB}-Gag p24 (Figure 5C). In addition, no. 157-4 sera from an HIV-1_{MNp}–infected animal was also weakly positive for their Env and Gag antigens. These animals showed intense plasma viral loads and enhanced proviral DNA copies in the spleen, BM, and thymus (Table 1), suggesting that hNOG mice inoculated with high doses of HIV and showing high rates of viral infection develop HIV-1–specific humoral immune responses that are analogous to those seen in human anti-HIV B-cell responses.

Discussion

Current small-animal models fall short of accurately mirroring human HIV-1 infection and thus have limited usefulness in analyzing the natural course of its progression to the disease state and in developing antiviral countermeasures. Although successful HIV-1 infections in immunodeficiency mice humanized with PBMCs have been reported,[12,13,21] transplanted human cells are soon depleted and do not elicit virus-specific immune responses, shedding little light on pathogenesis and vaccine development. By using NOG mice that received hematopoietic stem cell transplants showing high rates of viral infection, we demonstrated HIV-specific antibody responses and viral infection parameters, including the following: (1) similar levels of susceptibility to both R5- and X4-tropic HIV-1; (2) high levels of viremia stably observed over 40 days; (3) immunohistochemical detection of infected cells in various organs; and (4) a distinct tissue distribution for R5- versus X4-tropic HIV-1s.

Among $CD4^+$ T cells, CXCR4 antigen is primarily expressed on naive and CCR5 on activated or memory cells.[26] hu-PBL-SCID mice become susceptible to R5-tropic HIV-1 strains,[27] since T cells

Table 1. Comparison of viral RNA copies in plasma and HIV-DNA copies in the spleen, BM, and thymus from hNOG mice receiving low- and high-dose viral inoculations

Mouse ID no.	HIV strain	$TCID_{50}$	Time after inoculation, d	RNA viral copies/mL	CD4/CD8 ratio	HIV-DNA copies/10^6 human cells		
						Spleen	BM	Thymus
Low-dose viral inoculation group								
113-1	HIV-1_{JRCSF}	200	18	6 240	1.8	34 177	11 785	3 495
112-2	HIV-1_{JRCSF}	200	18	<500	1.2	< 100	< 100	< 100
113-2	HIV-1_{JRCSF}	200	40	6 177	1.6	25 855	27 920	3 473
112-3	HIV-1_{JRCSF}	200	40	<500	0.9	< 100	< 100	<100
112-4	HIV-1_{MNp}	180	18	72 477	1.3	18 873	100	ND
113-4	HIV-1_{MNp}	180	40	70 667	0.3	4 947	653	32 163
112-1	HIV-1_{MNp}	180	40	<500	0.9	< 100	< 100	< 100
High-dose viral inoculation group								
136-3	HIV-1_{JRCSF}	65 000	25	252 381	0.8	958 871	1 797 600	232 155
136-2	HIV-1_{JRCSF}	65 000	29	50 167	0.7	41 172	54 521	8 600
141-1	HIV-1_{JRCSF}	65 000	30	67 667	2.2	27 735	52 430	429
161-3	HIV-1_{JRCSF}	65 000	30	13 847	0.9	104 466	14 653	111 080
157-3	HIV-1_{MNp}	20 000	31	1 253 925	0.5	41 053	56 802	976 556
157-4	HIV-1_{MNp}	20 000	31	147 973	0.6	3 634	262	40 796
161-6	HIV-1_{MNp}	20 000	31	108 073	1.7	4 991	< 100	3 673

Seven mice inoculated with a low infectious dose of HIV-1_{JRCSF} (200 $TCID_{50}$) or HIV-1_{MNp} (180 $TCID_{50}$), and 7 mice receiving a high infectious dose of HIV-1_{JRCSF} (65 000 $TCID_{50}$) or HIV-1_{MNp} (20 000 $TCID_{50}$) were listed.

ND indicates not done.

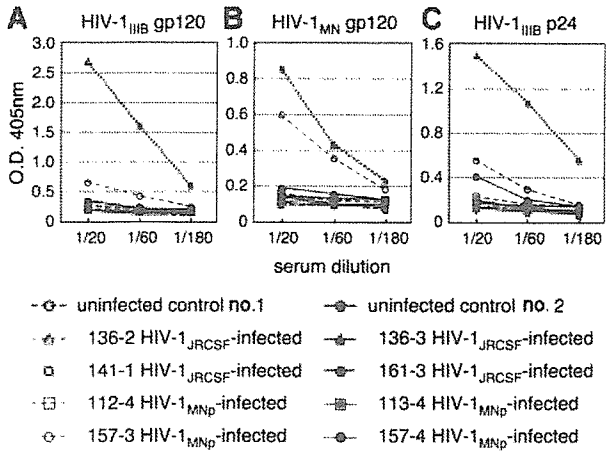

Figure 5. Detection of anti–HIV-1 antibodies from the plasma of HIV-1–infected mice. An ELISA assay was conducted by using plasma from 14 mice inoculated with either HIV-1_{JRCSF} or HIV-1_{MNp}, and from 2 uninfected control mice. Representatives (n = 8) of the 14 HIV-1–inoculated mice, and the 2 uninfected mice, are shown in the panels. Measurements of specific human antibodies for HIV-1_{IIIB} gp120 (A), HIV-1_{MN} gp120 (B), and HIV-1_{IIIB} p24 antigens (C) were shown. Results are expressed as the means from triplicate assays in 3 different experiments.

are initially activated in the xenogenic environment and then become anergic.[14] In contrast, SCID-hu (Thy/Liv) mice are more susceptible to X4 than to R5 strains[6] because HIV-1 infection is restricted mainly to the engrafted thymus that is primarily comprised of immature T cells, suggesting that this model may not be practical overt HIV infection. Our study represents the first attempt to infect NOG mice that received transplants of human hematopoietic stem cells with HIV-1. Very similar infection rates were seen for both R5 and X4 strains in the mouse model. Flow cytometry revealed both $CXCR4^+CD4^+$ and $CCR5^+CD4^+$ cells in PB, the spleen, and BM, but only CXCR4 on thymic $CD4^+$ T cells. It also showed the scattering of human macrophages, known to be susceptible to R5-tropic HIV-1 strains[28,29] and the source of HIV-1,[23,30-32] throughout various organs. $p24^+$ macrophage-like cells were detected in these organs after R5-tropic HIV-1_{JRCSF} infection. These data may help explain the susceptibility of hNOG mice to both R5- and X4-tropic HIV strains and also shed light on the active replenishment of these target cells in mice.

SCID mouse systems have been actively used in the evaluation of anti–HIV-1 drugs.[9,11,21] In most cases, HIV-1 detection levels reach a peak within a month after inoculation and level off, accompanied by $CD4^+$ T-cell depletion.[3,12,13] Although suitable for short-term experiments, it is also true that these models require large numbers of mice because of large variations in infection efficiency. In contrast, very stable infections were noted in our hNOG mice that were inoculated with a high dose of HIVs. They did not show rapid CD4/CD8 decrease in spite of high levels of viremia persisting for more than 40 days. Efficient hematopoiesis and thymopoiesis of human cells probably compensated for the loss of $CD4^+$ T cells, allowing for persistent infection. This capacity of the hNOG mouse system makes it attractive as a model for the long-term evaluation of anti–HIV-1 drugs. In addition to destroying mature blood cells, altered hematopoiesis in BM and the thymus has also been reported to be responsible for immunodeficiency in patients with AIDS.[33,34] To study hematopoietic abnormalities in HIV-1 infection, both SCID-hu (Thy/Liv) mice[8,35,36] and SIV- or SHIV-infected macaque models[20,37-39] have been used. The current hNOG mouse system, in which human cells are efficiently reproduced from stem cells and then settled into hematopoietic organs, offers a promising model for the study of events that occur after infection not only with R5-tropic HIV-1 but also with X4-tropic HIV-1. Indeed, the BM of hNOG mice infected with R5-tropic HIV-1 exhibited exceptionally elevated levels of HIV-DNA copies. On the other hand, the thymus of X4-tropic HIV-1_{MNp}–infected hNOG mice yielded large numbers of HIV-DNA copies, which seemed to correlate with the predominant expression of CXCR4 on the thymocytes. Thus, further observation is essential to address whether AIDS symptoms such as considerable $CD4^+$ T-cell depletion and hematopoietic abnormalities eventually occur in these mice.

It is noteworthy that human antibodies against both HIV-1 Env gp120 and Gag p24 antigens were detected in mice no. 136-3, no. 157-3, and no. 157-4 after exposure to high titers of HIV-1, suggesting that hNOG mice have the ability to respond to HIV-1 antigens. This encourages us to develop antibody-based HIV vaccine candidates, although additional modifications are required for the stable induction of immune responses. Importantly, since the seroconverted mice showed high viremia and high numbers of proviral DNA copies in the spleen, BM, and thymus, abundant viral production may stimulate human B-cell responses against HIV-1 and generate specific antibodies. These mice showed little or no detectable human IgG against HIV-1, as determined by Western blot analysis (data not shown), suggesting that very low levels of class-switching occurred in these mice, though further study is required.

In addition to the humoral immune responses, the induction of primary T-cell responses is critical for the study of HIV-specific immune responses and pathogenesis, as well as for vaccine development. Although we did not demonstrate the T-cell ability to respond to virus antigens, human T cells from the spleen proliferated when stimulated with anti–human CD3 antibodies (data not shown), indicating that the human T cells in the NOG mice that received transplants of hematopoietic stem cells are capable of responding to T-cell receptor–mediated signals and are expected to be able to elicit primary antigen-specific immune responses against foreign antigens. To address whether the specific T-cell responses may be induced will be one of the important studies.

In conclusion, the NOG mice that received transplants of human hematopoietic stem cells successfully achieved systemic and persistent infection with both R5-tropic and X4-tropic HIV-1, and generated humoral immune responses against HIV-1. These capacities of the hNOG mouse model may be very attractive for the study of HIV pathogenesis and humoral immune responses induced by HIV vaccine candidates.

Acknowledgments

We thank Yuetsu Tanaka of the University of Ryukyus, Tetsutaro Sata of NIID, and Shuzo Matsushita of Kumamoto University for their kind provision of mAbs to HIV-1, as well as Yukoku Tamaoka of Saiseikai Central Hospital, Toshio Akashi of Kumakiri Obstetric and Gynecologic Clinic, and Hideo Mugishima of Nihon University School of Medicine for their provision of umbilical cord blood. We also would like to express our gratitude to Ken Watanabe and Hideko Ogata of Tokyo Medical and Dental University for their skillful technical support.

This work was supported by grants from Research on Health Sciences focusing on Drug Innovation, the Japan Health Sciences Foundation.

Authorship

Contributions: S.W., K.T., N.S., M.H., and N.Y. designed the study; S.W., K.T., S.O., S.H., M.Y., Y.S., M.Z.D., and Z.Y. carried out the research; M.I. contributed live mice; S.W., K.T., and T.M. analyzed the data; N.S., M.H., and N.Y. controlled the data; S.W. wrote the paper; and all authors checked the final version of the manuscript.

Conflict-of-interest statement: The authors declare no competing financial interests.

Correspondence: Naoki Yamamoto, AIDS Research Center, National Institute of Infectious Diseases, 1-23-1 Toyama, Shinjuku-ku, Tokyo 162-8640, Japan; e-mail: nyama@nih.go.jp; Mitsuo Honda, AIDS Research Center, National Institute of Infectious Diseases, 1-23-1 Toyama, Shinjuku-ku, Tokyo 162-8640, Japan; e-mail: mhonda@nih.go.jp; and Norio Shimizu, Department of Virology, Division of Medical Science, Medical Research Institute, Tokyo Medical and Dental University, 1-5-45 Yushima, Bunkyo-ku, Tokyo 113-8519, Japan; e-mail: nshivir@tmd.ac.jp.

References

1. Letvin NL, Barouch DH, Montefiori DC. Prospects for vaccine protection against HIV-1 infection and AIDS. Annu Rev Immunol. 2002;20:73-99.
2. Namikawa R, Kaneshima H, Lieberman M, Weissman IL, McCune JM. Infection of the SCID-hu mouse by HIV-1. Science. 1988;242: 1684-1686.
3. Bonyhadi ML, Rabin L, Salimi S, et al. HIV induces thymus depletion in vivo. Nature. 1993; 363:728-732.
4. Aldrovandi GM, Feuer G, Gao L, et al. The SCID-hu mouse as a model for HIV-1 infection. Nature. 1993;363:732-736.
5. Su L, Kaneshima H, Bonyhadi M, et al. HIV-1-induced thymocyte depletion is associated with indirect cytopathogenicity and infection of progenitor cells in vivo. Immunity. 1995;2:25-36.
6. Kaneshima H, Su L, Bonyhadi ML, Connor RI, Ho DD, McCune JM. Rapid-high, syncytium-inducing isolates of human immunodeficiency virus type 1 induce cytopathicity in the human thymus of the SCID-hu mouse. J Virol. 1994;68:8188-8192.
7. Jenkins M, Hanley MB, Moreno MB, Wieder E, McCune JM. Human immunodeficiency virus-1 infection interrupts thymopoiesis and multilineage hematopoiesis in vivo. Blood. 1998;91:2672-2678.
8. Koka PS, Fraser JK, Bryson Y, et al. Human immunodeficiency virus inhibits multilineage hematopoiesis in vivo. J Virol. 1998;72:5121-5127.
9. Mosier DE, Gulizia RJ, Baird SM, Wilson DB, Spector DH, Spector SA. Human immunodeficiency virus infection of human-PBL-SCID mice. Science. 1991;251:791-794.
10. Torbett BE, Picchio G, Mosier DE. hu-PBL-SCID mice: a model for human immune function, AIDS, and lymphomagenesis. Immunol Rev. 1991;124: 139-164.
11. Ruxrungtham K, Boone E, Ford H Jr, Driscoll JS, Davey RT Jr, Lane HC. Potent activity of 2′-beta-fluoro-2′,3′-dideoxyadenosine against human immunodeficiency virus type 1 infection in hu-PBL-SCID mice. Antimicrob Agents Chemother. 1996;40:2369-2374.
12. Mosier DE, Gulizia RJ, MacIsaac PD, Torbett BE, Levy JA. Rapid loss of CD4+ T cells in human-PBL-SCID mice by noncytopathic HIV isolates. Science. 1993;260:689-692.
13. Koyanagi Y, Tanaka Y, Kira J, et al. Primary human immunodeficiency virus type 1 viremia and central nervous system invasion in a novel hu-PBL-immunodeficient mouse strain. J Virol. 1997; 71:2417-2424.
14. Tary-Lehmann M, Saxon A, Lehmann PV. The human immune system in hu-PBL-SCID mice. Immunol Today. 1995;16:529-533.
15. Ito M, Hiramatsu H, Kobayashi K, et al. NOD/SCID/gamma(c)(null) mouse: an excellent recipient mouse model for engraftment of human cells. Blood. 2002;100:3175-3182.
16. Yahata T, Ando K, Nakamura Y, et al. Functional human T lymphocyte development from cord blood CD34+ cells in nonobese diabetic/Shi-scid, IL-2 receptor gamma null mice. J Immunol. 2002; 169:204-209.
17. Hiramatsu H, Nishikomori R, Heike T, et al. Complete reconstitution of human lymphocytes from cord blood CD34+ cells using the NOD/SCID/gammacnull mice model. Blood. 2003;102:873-880.
18. Matsumura T, Kametani Y, Ando K, et al. Functional CD5+ B cells develop predominantly in the spleen of NOD/SCID/gammac(null) (NOG) mice transplanted either with human umbilical cord blood, bone marrow, or mobilized peripheral blood CD34+ cells. Exp Hematol. 2003;31:789-797.
19. Shinohara K, Sakai K, Ando S, et al. A highly pathogenic simian/human immunodeficiency virus with genetic changes in cynomolgus monkey. J Gen Virol. 1999;80:1231-1240.
20. Yamakami K, Honda M, Takei M, et al. Early bone marrow hematopoietic defect in simian/human immunodeficiency virus C2/1-infected macaques and relevance to advance of disease. J Virol. 2004;78:10906-10910.
21. Nakata H, Maeda K, Miyakawa T, et al. Potent anti-R5 human immunodeficiency virus type 1 effects of a CCR5 antagonist, AK602/ONO4128/GW873140, in a novel human peripheral blood mononuclear cell nonobese diabetic-SCID, interleukin-2 receptor gamma-chain-knocked-out AIDS mouse model. J Virol. 2005;79:2087-2096.
22. Heath SL, Tew JG, Tew JG, Szakal AK, Burton GF. Follicular dendritic cells and human immunodeficiency virus infectivity. Nature. 1995;377:740-744.
23. Orenstein JM, Fox C, Wahl SM. Macrophages as a source of HIV during opportunistic infections. Science. 1997;276:1857-1861.
24. van Kooyk Y, Geijtenbeek TB. A novel adhesion pathway that regulates dendritic cell trafficking and T cell interactions. Immunol Rev. 2002;186: 47-56.
25. Taylor JR Jr, Kimbrell KC, Scoggins R, Delaney M, Wu L, Camerini D. Expression and function of chemokine receptors on human thymocytes: implications for infection by human immunodeficiency virus type 1. J Virol. 2001;75:8752-8760.
26. Bleul CC, Wu L, Hoxie JA, Springer TA, Mackay CR. The HIV coreceptors CXCR4 and CCR5 are differentially expressed and regulated on human T lymphocytes. Proc Natl Acad Sci U S A. 1997; 94:1925-1930.
27. Fais S, Lapenta C, Santini SM, et al. Human immunodeficiency virus type 1 strains R5 and X4 induce different pathogenic effects in hu-PBL-SCID mice, depending on the state of activation/differentiation of human target cells at the time of primary infection. J Virol. 1999;73:6453-6459.
28. Gartner S, Markovits P, Markovitz DM, Kaplan MH, Gallo RC, Popovic M. The role of mononuclear phagocytes in HTLV-III/LAV infection. Science. 1986;233:215-219.
29. Koyanagi Y, Miles S, Mitsuyasu RT, Merrill JE, Vinters HV, Chen IS. Dual infection of the central nervous system by AIDS viruses with distinct cellular tropisms. Science. 1987;236:819-822.
30. Gendelman HE, Orenstein JM, Baca LM, et al. The macrophage in the persistence and pathogenesis of HIV infection. AIDS. 1989;3:475-495.
31. Embretson J, Zupancic M, Ribas JL, et al. Massive covert infection of helper T lymphocytes and macrophages by HIV during the incubation period of AIDS. Nature. 1993;362:359-362.
32. Igarashi T, Brown CR, Endo Y, et al. Macrophage are the principal reservoir and sustain high virus loads in rhesus macaques after the depletion of CD4+ T cells by a highly pathogenic simian immunodeficiency virus/HIV type 1 chimera (SHIV): implications for HIV-1 infections of humans. Proc Natl Acad Sci U S A. 2001;98:658-663.
33. Mir N, Costello C, Luckit J, Lindley R. HIV-disease and bone marrow changes: a study of 60 cases. Eur J Haematol. 1989;42:339-343.
34. Moses A, Nelson J, Bagby GC Jr. The influence of human immunodeficiency virus-1 on hematopoiesis. Blood. 1998;91:1479-1495.
35. Koka PS, Jamieson BD, Brooks DG, Zack JA. Human immunodeficiency virus type 1-induced hematopoietic inhibition is independent of productive infection of progenitor cells in vivo. J Virol. 1999;73:9089-9097.
36. Koka PS, Kitchen CM, Reddy ST. Targeting c-Mpl for revival of human immunodeficiency virus type 1-induced hematopoietic inhibition when CD34+ progenitor cells are re-engrafted into a fresh stromal microenvironment in vivo. J Virol. 2004;78: 11385-11392.
37. Hillyer CD, Lackey DA 3rd, Villinger F, Winton EF, McClure HM, Ansari AA. CD34+ and CFU-GM progenitors are significantly decreased in SIVsmm9 infected rhesus macaques with minimal evidence of direct viral infection by polymerase chain reaction. Am J Hematol. 1993;43:274-278.
38. Thiebot H, Louache F, Vaslin B, et al. Early and persistent bone marrow hematopoiesis defect in simian/human immunodeficiency virus-infected macaques despite efficient reduction of viremia by highly active antiretroviral therapy during primary infection. J Virol. 2001;75:11594-11602.
39. Thiebot H, Vaslin B, Derdouch S, et al. Impact of bone marrow hematopoiesis failure on T-cell generation during pathogenic simian immunodeficiency virus infection in macaques. Blood. 2005; 105:2403-2409.